Research Paper

Molecular characterization of ferroptosis in soft tissue sarcoma constructs a prognostic and immunotherapeutic signature through experimental and bioinformatics analyses

Zhi-Qiang Yang[1,*], Liang-Yu Guo[1,*], Kang-Wen Xiao[1,3,*], Chong Zhang[2], Min-Hao Wu[1], Fei-Fei Yan[1], Lin Cai[1]

[1]Department of Orthopedics, Zhongnan Hospital of Wuhan University, Wuhan, Hubei 430071, People's Republic of China
[2]Department of Orthopedics, Renmin Hospital of Wuhan University, Wuhan, Hubei 430071, People's Republic of China
[3]School of Medicine, Washington University, St. Louis, MO 63110, USA
[*]Equal contribution

Correspondence to: Fei-Fei Yan, Lin Cai; **email:** yanfeifei0120@whu.edu.cn, orthopedics@whu.edu.cn
Keywords: ferroptosis, soft tissue sarcoma, immunotherapy, nomogram, survival analysis
Received: June 12, 2023 **Accepted:** October 2, 2023 **Published:** October 20, 2023

ABSTRACT

Ferroptosis regulators have been found to affect tumor progression. However, studies focusing on ferroptosis and soft tissue sarcoma (STS) are rare. Somatic mutation, copy number variation, reverse transcription-quantitative polymerase chain reaction (RT-qPCR) analysis, consensus clustering, differentially expressed genes analysis (DEGs), principal component analysis (PCA) and gene set enrichment analysis (GSEA) were used to identify and explore different ferroptosis modifications in STS. A nomogram was constructed to predict the prognosis of STS. Moreover, three immunotherapy datasets were used to assess the Fescore. Western blotting, siRNA transfection, EdU assay and reactive oxygen species (ROS) measurement were performed. 16 prognostic ferroptosis regulators were screened and significant differences were observed in somatic mutation, copy number variation (CNV) and RT-qPCR among these ferroptosis regulators. 2 different ferroptosis modification patterns were found (Fe cluster A and B). Fe cluster A with higher Fescore was correlated with p53 pathway and had better prognosis of STS (p = 0.002) while Fe cluster B with lower Fescore was correlated with angiogenesis and MYC pathway and showed a poorer outcome. Besides, the nomogram effectively predicted the outcome of STS and the Fescore could also well predict the prognosis of other 16 tumors and immunotherapy response. Downregulation of LOX also inhibited growth and increased ROS production in sarcoma cells. The molecular characterization of ferroptosis regulators in STS was explored and an Fescore was constructed. The Fescore quantified ferroptosis modification in STS patients and effectively predicted the prognosis of a variety of tumors, providing novel insights for precision medicine.

INTRODUCTION

With multiple subtypes and different clinical outcomes, STS has attracted researchers' attention in the recent years [1]. Being a rare tumor, STS accounted for 0.71% of estimated new cases based on the latest cancer statistics in United States [2]. According to different origin and morphology, STS can be also divided into liposarcoma, hemangioma, neuroma, etc. At present, the main treatment of soft tissue sarcoma is surgery resection combined with radiology therapy, which reduces the risk of reoccurrence [3]. However,

the probability of STS patients being alive at 5 years is only 10% [4]. Therefore, exploring new targets and implementing individualized treatment is of great significance to improve the prognosis of STS patients.

Ferroptosis is characterized by the iron dependent accumulation of lipid peroxidation to a lethal level [5]. Recent studies have revealed a close relationship between ferroptosis and tumor progression. Ferroptosis regulator HSPB1 was also related to decreased ferroptosis by reducing the expression of TFR1, which further accelerated cervical carcinoma growth [6]. Another research revealed that rhabdomyosarcoma cells death was induced by Erastin through lipid peroxidation and reactive oxygen species production, which were typical features of ferroptosis [7]. Besides, recent research showed that ME1 absence could lead to synovial sarcoma cells being more sensitive to ferroptotic cell death [8]. Moreover, desmoid-type fibromatosis cells death could be induced by sorafenib through ferroptosis [9]. Considering the close relationship between ferroptosis and the progression of STS and other tumors, it is very necessary to further explore the ferroptosis modification patterns in STS.

Since the advent of immunotherapy, it has been of wide interest to clinicians and scientists all over the world. Immunotherapy mainly included PD-1/PD-L1 and CTLA-4, which were also called immune checkpoint blockade (ICB) [10]. Although ICB has made good achievements against cancer, only a small number of patients could respond to ICB, and the price of treatment was expensive, which greatly limited the use of ICB [11]. Tumor microenvironment (TME); microenvironment around tumor cells, also plays an important role in regulating the outcome of immunotherapy. A recent study reported that PD-L1 could be regulated by Interferon γ in vascular endothelial cell [12]. Besides, interleukin-17 (IL-17) in the TME could also increase the expression of PD-L1 in prostate cancer and colon cancer, which further affected immunotherapy response [13]. A previous study also revealed that transforming growth factor beta (TGF-β) could enhance the expression of PD-1/L1 in hepatocellular carcinoma [14]. Although the relationship between TME and tumor immunotherapy have been discussed, these studies were not associated with ferroptosis. Hence, it was imperative to explore the modification pattern of ferroptosis in STS and identify novel predictive markers for immunotherapy response.

Recently we explored the role of N6-methyladenosine modification in STS [15]. Based on this experience, here 16 prognostic ferroptosis regulators were screened through univariate Cox regression analysis. RT-qPCR, somatic mutation and copy number variation further revealed significant differences of these regulators in STS. Two ferroptosis modification patterns were identified using consensus clustering [16]. Moreover, significant differences in immune infiltration and prognosis between the ferroptosis modification patterns were observed by CIBERSORT, ESTIMATE and survival packages [17]. Hence, we constructed an Ferroptosis-related score (Fescore), which well predicted the immune infiltration and prognosis of STS. The Fescore could also predict the response to ICB, which provided new insights for precision medicine and targeted therapy.

MATERIALS AND METHODS

Sample collection and data processing

In this study, 33 types of cancer and the corresponding survival information in The Cancer Genome Atlas (TCGA) were downloaded from UCSC-XENA (http://xena.ucsc.edu/). The somatic mutation and CNV of TCGA-SARC (n = 265) were also obtained from UCSC-XENA. Sarcoma datasets GSE17674 [18], undifferentiated sarcoma (GSE119041 [19]), Liposarcoma (GSE159848 [20]), Leiomyosarcoma (GSE159847 [20]), Synovial Sarcoma (GSE40021 [21]), Ewing Sarcoma (GSE17168 [18]), and Fibrosis sarcoma (GSE71118 [22]) were collected from Gene Expression Omnibus (GEO) database. GPL570 platform was used for GSE17674, GSE17618 and GSE71118 while gencode platform (https://www.gencodegenes.org/) was used for 33 types of cancer in TGCA. GPL6480 platform was used for GSE159848, GSE40021 and GSE159847. GPL17692 platform was used for GSE119041. Robust multi-array average (RMA) normalization was applied in GSE17674 and GSE17618 and Transcripts Per Kilobase Million (TPM) normalization was performed in 33 types of cancer. GCRMA algorithm was applied in GSE71118 and Quantile algorithm was applied in GSE159848, GSE40021 and GSE159847. Data from GSE119041 were normalized with the default settings on Thermo Fishers Expression Console 1.4.1.46 Software.

Three immunotherapy datasets IMvigor210 [18] (n = 298), GSE78220 (n = 28) and GSE35640 (n = 65) were collected from recent studies. IMvigor210, GSE78220 and GSE35640 were normalized by trimmed mean of M-values, FPKM (Fragments Per Kilobase Million) and RMA, respectively. Ferroptosis regulators were screened according to recent research [23]. Samples without full clinical characteristics were excluded from this study. Three STS samples and the corresponding normal tissue were obtained from Department of Orthopedics, Zhongnan Hospital of Wuhan University. Detailed information of these datasets was shown in Supplementary Table 1. The list of ferroptosis regulators was shown in Supplementary Table 2. The flowchart was shown in Figure 1.

LOX knockdown using siRNA transfection

A siRNA strategy was used to knock down LOX in HT1080 and A204 cells. Briefly, 1 × 10^5 cells were added to fresh medium without antibiotics and seeded in six-well plates 24 hrs before transfection. For transfection, all siRNAs (si-LOX or the negative control, siNC) (Tsingke Biotechnology Co., Ltd., Beijing, China) were resuspended at a concentration of 20 μM and then transfected into HT1080 and A204 cells. TSnanofect V1 transfection reagent (Tsingke Biotechnology) was used when the cells reached 50–70% confluence. A transfection rate of 70–85% of cells was used for further experiments. The siRNA sequences targeting LOX were shown in Supplementary Table 3.

Western blotting

HT1080 and A204 cells were seeded in 6-well plates, and then transfected with NC group and Si group respectively for 48 hours and then collected. Cells were washed once with PBS and then lysed with Protein Lysis Buffer containing protease and phosphatase inhibitor cocktail for 30 min on ice. Cell lysates were centrifuged at 12,000 × g for 15 min at 4°C, and the supernatant was collected. Protein concentration was quantified using the BSA protein assay according to the manufacturer's instructions. Equal amounts of total protein were separated by SDS-PAGE (8–12%) at 80–120 V for 1.5 h and transferred to a 0.45 μM PVDF membrane at 230 mA for 1.5 h. After blocking with 5%

Figure 1. The flowchart of this study.

skim milk in TBST buffer for 1 h at room temperature, membranes were incubated with primary antibodies anti-GAPDH and ant-LOX (GAPDH, LOX antibodies were purchased from ProteinTech (Wuhan, China)) overnight at 4°C. Membranes were washed three times with TBST buffer and then incubated with peroxidase-conjugated secondary antibodies for 1 h at room temperature. Specific antibody binding was detected by a chemiluminescence kit.

EdU assay

EdU assay was performed using the EdU–555 Cell Proliferation Assay Kit (Beyotime, Shanghai, China). Observation and photography were performed using a fluorescence microscope (Olympus, Tokyo, Japan).

ROS

To assess the intracellular ROS scavenging activity, the cells were stained with the fluorescent 2,7-dichloro-dihydrofluorescein diacetate (DCFH-DA) probe with ROS assay kit as previously described [24]. In short, HT1080 and A204 cells were harvested and collected 48 hours after transfection, and washed with serum free medium. Then, the cells were combined with 10 μ M DCFH-DA probes (Molecular Probes, Eugene, OR, USA) and were mixed in serum-free medium and incubated in 37°C darkness for 30 minutes, with slight stirring every 5 minutes. Then, we collected the cell granules, washed them with PBS three times, and BS is used for flow cytometry analysis. Induced green fluorescent nanoparticles from 10000 cells were recorded at 488 nm. FlowJ software was used to analyze the average fluorescence intensity.

Transwell assays

A Transwell assay was performed using a Transwell system (24 wells, 8 μm pore size with poly-carbonate membrane) according to the manufacturer's instructions. First, HT1080 and A204 cells were seeded into the upper chamber with serum-free corresponding medium. Medium with 10% FBS was put into the lower compartment, and the cells were allowed to migrate for 48 h. The remaining cells in the upper chamber were scraped out by a cotton swap. Cells were fixed with ice-cold methanol and stained with 0.1% crystal violet solution. The number of cells that migrated to the lower side was counted in five randomly selected fields under a light microscope. The cell number was counted and analyzed statistically.

Cell line, RNA extraction and RT-qPCR

Human skeletal muscle cell line (HSMC) and sarcoma cell line (A673) were purchased from the American Type Culture Collection (Manassas, VA, USA). Human fibrosarcoma cell line HT1080 and rhabdomyosarcoma cell line A204 were purchased from Procell (Wuhan, China). A673 and HSMC were cultured in RPMI 1640 medium (Hyclone, Logan, UT, USA) and DMEM (Hyclone) respectively. HT-1080 and A204 were cultured in MEM (Procell) and McCoy's 5A medium (Procell). All complete media were supplemented with 10% fetal bovine serum (Gibco, Langley, OK, USA) and 1% anti-biotics (100 U/mL penicillin, 100 μg/mL streptomycin). The cells were maintained in an incubator with 37°C and 5% CO2. The total RNA of cell lines and tissue was extracted by Trizol method (Invitrogen, Waltham, MA, USA), and then the RNA was reverse transcribed by reverse transcription kit (Roche, Basel, Switzerland) to obtain cDNA; RT-qPCR was performed according to the instructions. The prime sequences of all genes were listed in Supplementary Table 4.

Identification of different ferroptosis modification patterns in STS through consensus clustering analysis

Prognostic ferroptosis regulators were screened using survival and survminer packages [25]. Then different ferroptosis modification patterns were calculated through consensus clustering analysis according to the expression of these 16 prognostic ferroptosis regulators. The above analysis was performed 1000 times to achieve stable clustering by ConsensusClusterPlus package.

Differentially expressed genes analysis and connectivity map analysis

DEGs were performed between different ferroptosis modification patterns by limma package [26]. Benjamini-Hochberg procedure was performed to adjust multiple hypothesis [27]. The requirement for DEGs was: adjust $p < 0.050$ and $\log^{FC} > 1$ or $\log^{FC} < -1$. Connectivity Map (cMap) was applied to reveal the functional relationship between small molecule compounds, genes and disease status [28]. The above DEGs were subsequently used for cMap analysis to explore potential drugs for STS. $p < 0.05$ indicated statistical significance.

Immune cell infiltration in STS

The CIBERSORT algorithm was used to explore the immune infiltration in STS samples. LM22 signature was used here and the permutation was set to 1000. Then ESTIMATE package was further applied to calculate the STS purity score [29].

Functional enrichment analysis

The 16 prognostic ferroptosis regulators were used for Gene Ontology (GO) analysis by clusterProfiler

package [30]. Significant pathways between different ferroptosis modification patterns were also identified using gene set enrichment analysis (GSEA) [31]. False discovery rate (FDR) < 0.05 was considered significant.

Construction of the Fescore and prognostic nomogram

To quantify the ferroptosis modification patterns in STS, an Fescore was constructed according to previous experience [32]. Detailed process of calculating Fescore was as follows: First, the DEGs between different ferroptosis modification patterns were used for consensus clustering analysis. Then Cox regression was performed to screen prognostic DEGs. Finally, PCA was performed to establish the Fescore on the basis of prognostic DEGs after z-score standardization and principal component 1 was regarded as signature score. The formula of Fescore is shown below:

$$Fescore = \sum pc1_m - \sum pc1_n$$

m was prognostic DEGs with Hazard Ratio (HR) < 1 while n was prognostic DEGs with HR > 1.

Besides, the prognostic nomogram to predict the survival of STS was constructed based on gender, age, race, metastatic status, margin status and Fescore by rms package (https://hbiostat.org/R/rms/). Bootstrap method was used with 1000 iterations and the calibration curves of survival of STS were also used to assess the predictive function of the nomogram.

Statistical analysis

Statistical Product and Service Solutions software (SPSS 22.0) and R 3.6.2 were used for data analysis. The somatic mutation of STS was displayed using maftool package [33]. The relative location of 16 prognostic ferroptosis regulators in human chromosome was shown by Rcircos package [34]. The relationship between different ferroptosis regulators and different immune cells were displayed by corrplot package, respectively [35]. Cox regression analysis [36] was used to explore prognostic ferroptosis regulators, prognostic DEGs and evaluate the prognostic value in other 32 types of cancer in TCGA. Survival package and survminer package were used for survival analysis and setting cut-off point. The heatmaps were drawn by Pheatmap package [37]. Log-rank test was used to compare the survival rate. The receiver operating characteristic (ROC) curve for predicting the prognosis of STS and immune response were performed by using timeROC package and pROC package, respectively. FactoMineR package [38] was used for PCA. Protein-protein interaction analysis was performed and visualized by STRING and cytoscape [39], respectively and hub genes were identified based on degree > 4. Kruskal-Walls test was used to compare differences among different clusters and groups. $p < 0.05$ was considered significant.

RESULTS

Overview of prognostic ferroptosis regulators variation in STS

A total of 60 ferroptosis regulators were screened according to a recent research [23]. After univariate Cox analysis of these 60 regulators in STS, a total of 16 regulators were significantly related to the prognosis of STS and were used for subsequent analysis. The result of univariate Cox regression analysis for prognostic ferroptosis regulators was shown in Figure 2A. A total of 16 ferroptosis regulators were considered to be closely related to the prognosis of STS: SQLE ($p < 0.001$), NFE2L2 ($p < 0.001$), GSS ($p < 0.001$), HSPB1 ($p = 0.0013$), NCOA4 ($p = 0.002$), HMGCR ($p = 0.0027$), CBS ($p = 0.0063$), AIFM2 ($p = 0.0065$), CRYAB ($p = 0.021$), NQO1 ($p = 0.021$), FANCD2 ($p = 0.024$), RPL8 ($p = 0.027$), ACSF2 ($p = 0.029$), ACACA ($p = 0.031$), CD44 ($p = 0.031$), SLC1A5 ($p = 0.033$). Then we explored the somatic mutation of these prognostic ferroptosis regulators and the results were shown in Figure 2B–2D. The main variant classification and type of somatic mutation in STS were missense mutation and single nucleotide polymorphism, respectively. Besides, 6 STS samples had ferroptosis-related mutations, accounting for 2.58% of the total STS samples ($n = 237$). The result of CNV analysis for these ferroptosis regulators was also shown in Figure 2E. CNV widely existed in these ferroptosis regulators. Among them, AIFM2 (56%), NCOA4 (48%) and CRYAB (47%) showed a higher frequency of CNV gain while GSS (40%), SQLE (32%) and RPL8 (30%) exhibited more CNV loss. We further analyzed the relationship between gene expression and CNV and the results were shown in Supplementary Figure 1. CNV was positively correlated with the expression of ferroptosis regulators. The relative location of 16 ferroptosis regulators was also marked in Supplementary Figure 2 and the correlation among these ferroptosis regulators was shown in Figure 3A. Many ferroptosis regulators had significant linear correlations with other ferroptosis regulators at gene expression level. Since huge differences of these ferroptosis regulators were detected in STS through somatic mutation and CNV analysis, we further explored their expression differences between STS and normal skeletal tissue based on public database GSE17674 (Figure 3B). The results of PCA and sample correlation heatmap also showed that ferroptosis could well differentiate the normal and tumor samples (Supplementary Figure 3). The result turned out that most ferroptosis regulators showed

significant expression differences. GO functional enrichment analysis was also performed and the result was shown in Figure 3C. The ferroptosis regulators were enriched in response to oxidative stress ($p < 0.001$) and aging ($p < 0.001$). To further explore the trend of these ferroptosis regulators and their potential meaning, we also performed the functional enrichment analysis of ferroptosis regulators that were significantly increased in tumor and normal tissues, respectively. The results showed that ferroptosis regulators up-regulated in tumor

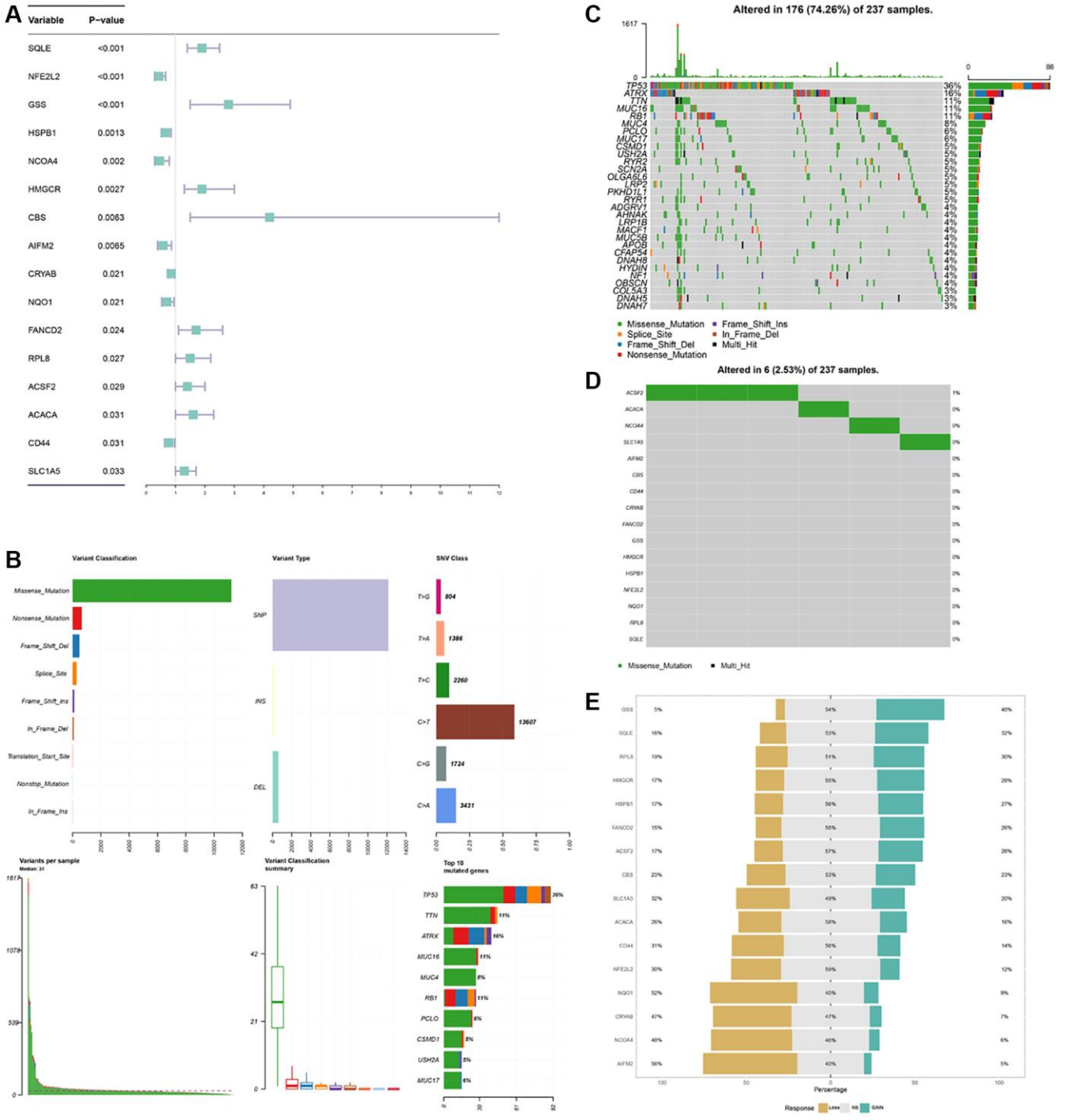

Figure 2. Landscape of prognostic difference, somatic mutations, CNV of ferroptosis regulators in STS. (**A**) Univariate Cox regression analysis for each ferroptosis regulators in STS. (**B**) Variant classifications of mutations in STS. (**C**) Summary of somatic mutations in STS. (**D**) Summary of somatic mutations of ferroptosis regulators in STS. (**E**) CNV of 16 ferroptosis regulators in STS.

tissues were mainly enriched in cholesterol biosynthetic process while ferroptosis regulators up-regulated in normal tissues were mainly enriched in response to oxidative stress (Supplementary Figure 4 and Supplementary Table 5). Moreover, the RT-qPCR was also performed to explore the expression difference of ferroptosis regulators at tissue and cell line levels and the result was shown in Figure 4 and Supplementary Figure 5. Similarly, compared with normal adjacent tissue, ferroptosis regulators exhibited significant expression differences in STS. The above results indicated that ferroptosis had a wide range of differential expression and variation in STS and different ferroptosis modification might regulate the clinical outcome and progression of STS.

Identification of 2 ferroptosis modification patterns through consensus clustering analysis

To further explore the role of ferroptosis in STS, 2 ferroptosis modification patterns (Fe cluster A and B) were identified through consensus clustering analysis based on the expression of these 16 ferroptosis regulators (Figure 5A). Fe cluster A had 134 samples while Fe cluster B had 131 samples. The expression of 16 ferroptosis regulators between different ferroptosis modification patterns was displayed as heatmap in Figure 5B. AIFM2 (p = 0.004), CRYAB (p < 0.001), HMGCR (p = 0.003), HSPB1 (p < 0.001), NFE2L2 (p = 0.001), NQO1 (p = 0.003), SLC1A5 (p < 0.001) and SQLE (p < 0.001) were considered significantly differentially expressed between these 2 clusters. PCA also suggested a good clustering effect (Figure 5C). Then survival analysis was performed between Fe cluster A and B and the result was shown in Figure 5D. Compared with Fe cluster B, Fe cluster A showed a significantly better prognosis of STS (p = 0.0018). Considering the huge prognostic differences between these 2 clusters, GSEA was further used to explore potential pathways between different ferroptosis modification patterns and the results were shown in Figure 5E–5I. All enriched pathways were shown in Supplementary Tables 6, 7. Fe cluster A was correlated with α interferon (Enrichment score (ES) = 0.50, FDR = 0), γ interferon (ES = 0.36, FDR = 0.001) and p53 pathway (ES = 0.27, FDR = 0.034) while WNT signaling (ES = −0.54, FDR = 0) and angiogenesis (ES = −0.55, FDR = 0) were related to Fe cluster B. These results were consistent with the result of survival analysis, which also proved that different ferroptosis modification patterns affected the prognosis of STS significantly.

Exploration of immune infiltration between different ferroptosis modification patterns in STS

In order to explore the role of ferroptosis in TME infiltration, a key factor regulating tumor immunotherapy, general immune infiltration of STS samples from TCGA-SARC were displayed in Supplementary Figure 6. Moreover, the 22 immune cells infiltration of different ferroptosis modification were shown in Figure 6A. Among them, dendritic resting cells (p < 0.05), eosinophils (p < 0.05), CD8 T cells (p < 0.05) were found to have a higher expression in Fe cluster A. Meanwhile, mast resting cells (p < 0.0001), M0 (p < 0.01) and M2 macrophages (p < 0.05) were highly expressed in Fe cluster B. The correlation plot of these 22 immune cells were also displayed in Figure 6B. Besides, the immune score and stromal score

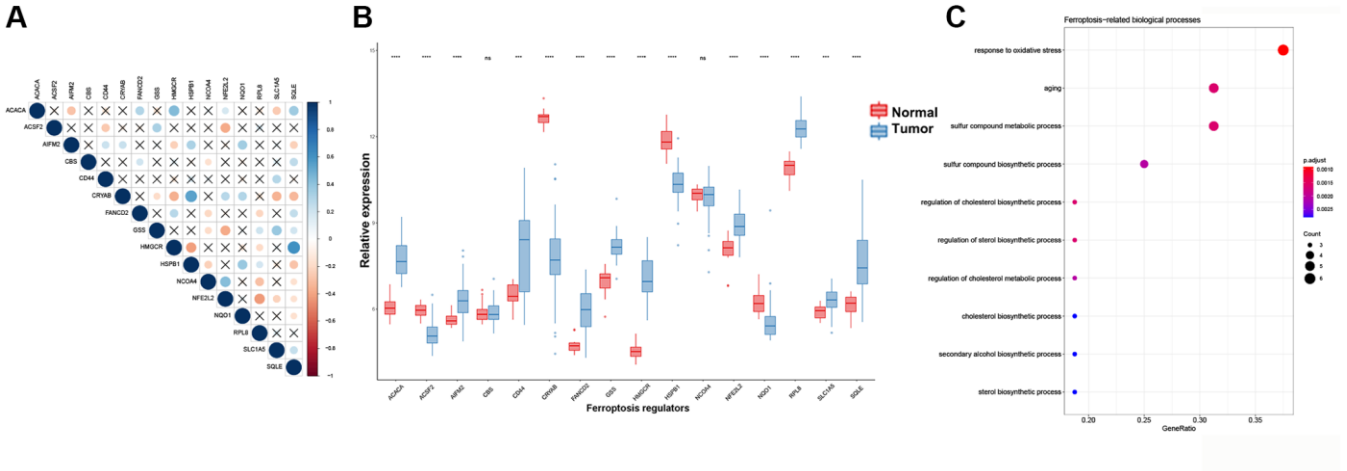

Figure 3. Expression, interactions and functional annotations of ferroptosis regulators in STS. (**A**) Correlation plot among 16 regulators using Pearson correlation analysis. PPI analysis of ferroptosis regulators. (**B**) Expression of different ferroptosis regulators between normal samples and STS samples in GSE17674. (**C**) Functional annotations for 16 ferroptosis regulators. $^{*}p$ < 0.05, $^{**}p$ < 0.01, $^{***}p$ < 0.001, $^{****}p$ = 0. Abbreviation: ns: no significance.

of different ferroptosis modification were calculated. In Figure 6C, there was no significant difference in immune scores between the two ferroptosis modification patterns. In Figure 6D, the stromal score between two ferroptosis modification patterns showed statistically significant (p = 0.004). Moreover, the survival curve for different immune/stromal score in different ferroptosis modification patterns were displayed in Figure 6E, 6F. Different immune score/ stromal score showed significant prognostic differences in different ferroptosis modification patterns (p < 0.0001). The above results revealed that different ferroptosis modification patterns affected the STS microenvironment and had a significant impact on the prognosis of STS.

Establishment of the Fescore

In order to further verify the stability of consensus clustering in STS, DEG analysis was performed between two Fe clusters and the result was shown in Figure 7A. 125 genes were upregulated in Fe cluster A while 49 genes were upregulated in Fe cluster B. The full list of these DEGs were shown in Supplementary Table 8. Functional enrichment analysis was performed based on these DEGs and the results showed that these DEGs were enriched in oxidoreductase activity-related pathways, which was necessary for ferroptosis occurrence (Supplementary Figure 7 and Supplementary Table 9). The heatmap of these DEGs

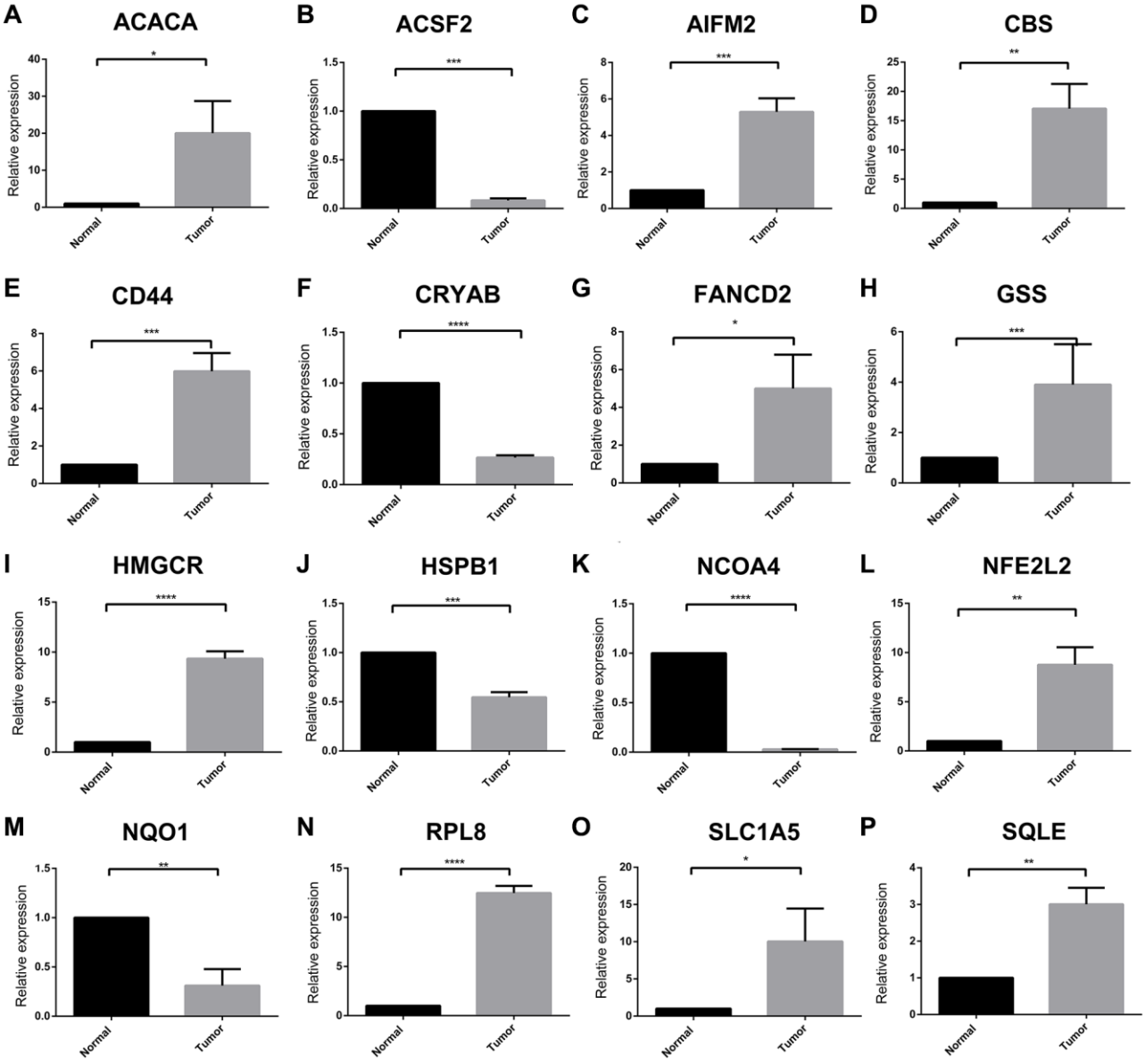

Figure 4. Expression of each ferroptosis regulators between STS and adjacent tissue by RT-qPCR. (**A**–**P**) The relative expression of ACACA, ACSF2, AIFM2, CBS, CD44, CRYAB, FANCD2, GSS, HMGCR, HSPB1, NCOA4, NFE2L2, NQO1, RPL8, SLC1A5 and SQLE between tumor and normal tissues, respectively. $^{*}p < 0.05$, $^{**}p < 0.01$, $^{***}p < 0.001$, $^{****}p = 0$. Abbreviation: ns: no significance.

was also displayed in Figure 7B. These DEGs were further used for cMap analysis and the results were shown in Supplementary Table 10. Among them, sulfadimethoxine ($p < 0.001$) and withaferin A ($p = 0.016$) might be potential targets treating STS. Then, consensus clustering analysis was performed based on the expression of these 174 DEGs and the results were shown in Figure 7C, 7D. Similarly, STS samples were divided into 2 new clusters (gene cluster A and B). Gene cluster A had 95 samples while gene cluster B had 170 samples. After comparing the results of two consensus clustering, 96.8% of samples from gene cluster A were found in Fe cluster A while 75.3% of samples from gene cluster B were also found in

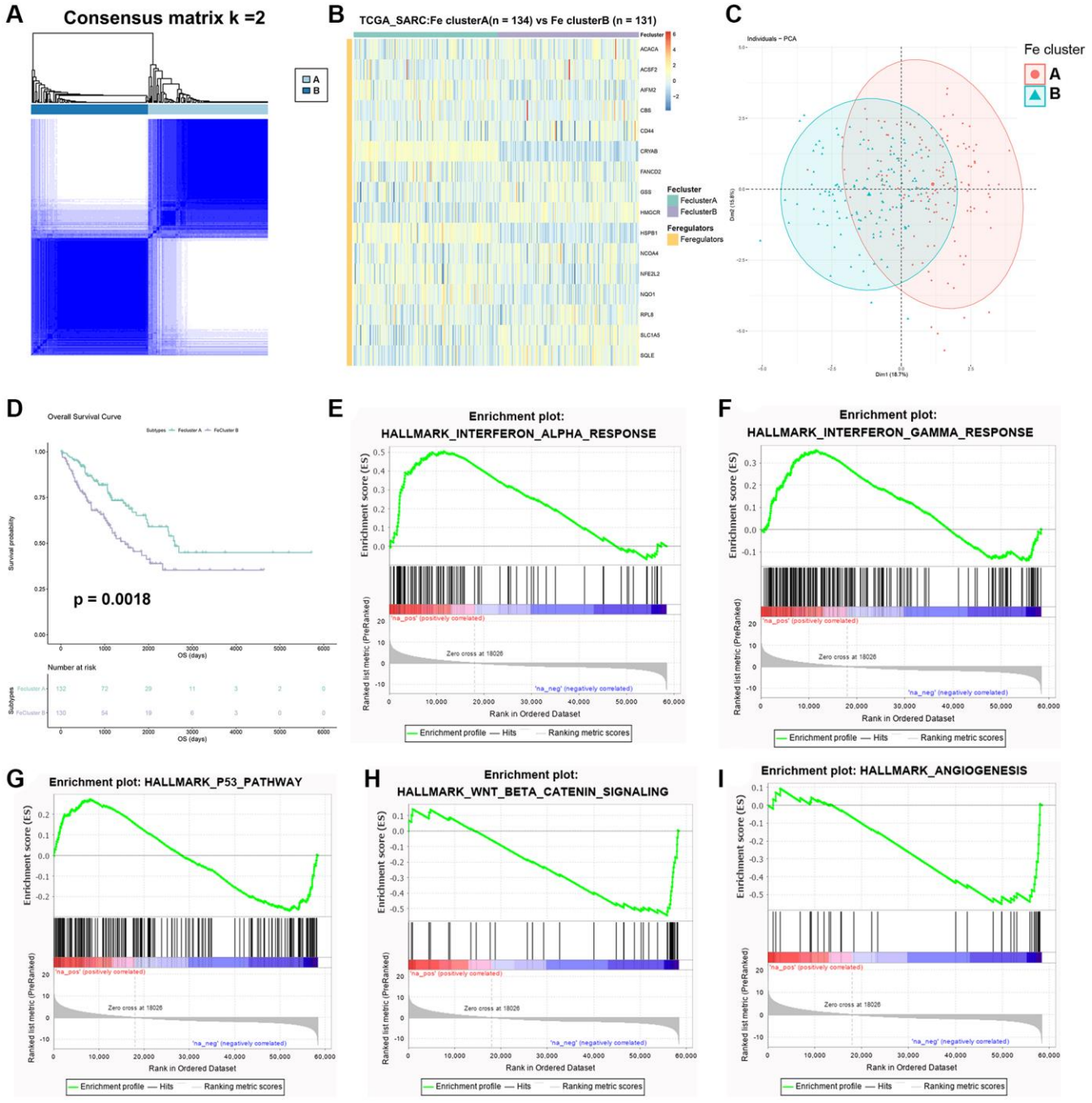

Figure 5. Identification of two ferroptosis modification patterns in STS. (**A**) The result of consensus clustering analysis in STS. (**B**) Heatmap of expression of 16 ferroptosis regulators in Fe clusters A and B. (**C**) The result of PCA of two Fe clusters. (**D**) Survival plot of two clusters in TCGA-SARC ($p = 0.0018$). (**E**) Enriched pathways in Fe cluster A: α interferon response. (**F**) Enriched pathways in Fe cluster A: γ interferon response. (**G**) Enriched pathways in Fe cluster A: p53 pathway. (**H**) Enriched pathways in Fe cluster B: WNT signaling. (**I**) Enriched pathways in Fe cluster B: angiogenesis.

Fe cluster B. These results indicated that our clustering result was relatively reliable. Further, the survival analysis between gene cluster A and B was performed (Figure 7E). Gene cluster A showed a better clinical outcome than gene cluster B (p = 0.0024). Besides, 174 DEGs were used for univariate Cox regression analysis to screen prognostic DEGs. A total of 43 prognostic DEGs were identified and the result was shown in

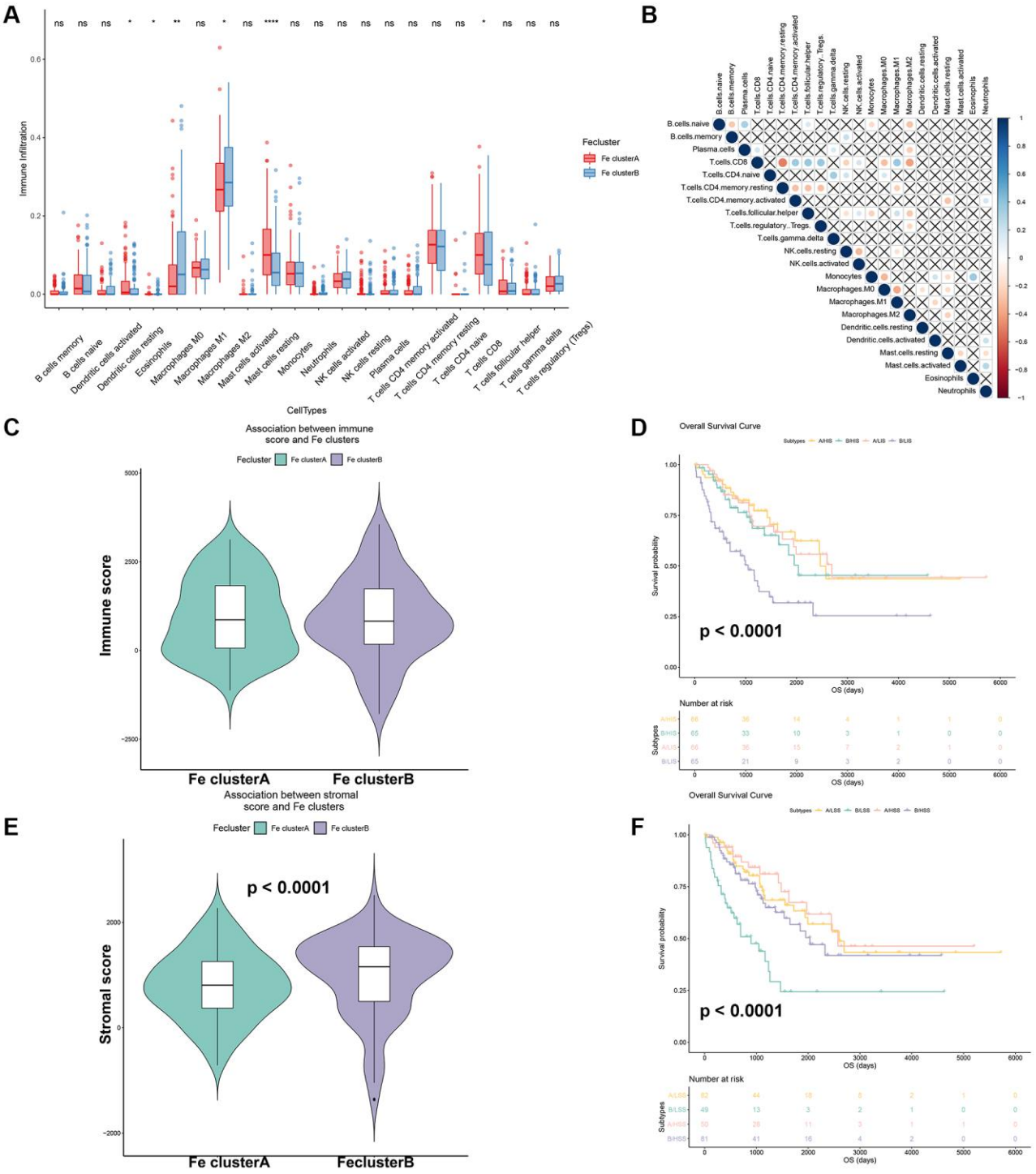

Figure 6. Effects of different ferroptosis modification patterns on immune infiltration of STS. (**A**) Comparison of immune cells-infiltration among Fe clusters A and B. (**B**) Correlation plot of each immune cells in TCGA-SARC. (**C**) Comparison of immune score among Fe clusters A and B. (**D**) Survival analysis of different immune scores among Fe clusters A and B (A: Fe cluster A, B: Fe cluster B, Abbreviations: LSS: Low immune score; HSS: High immune score); (**E**) Comparison of stromal scores among Fe clusters A and B. (**F**) Survival analysis of different stromal scores among Fe clusters A and B. (A: Fe cluster A, B: Fe cluster B, Abbreviations: LIS: Low stromal score; HIS: High stromal score); $^{*}p < 0.05$, $^{**}p < 0.01$.

Supplementary Table 11. Then the Fescore of each STS sample was calculated through PCA and the results were shown in Figure 7F, 7G. Fe cluster A exhibited a significantly higher Fescore than Fe cluster B (p < 0.001). Similarly, gene cluster A also had a significantly higher Fescore than gene cluster B (p < 0.001). After STS samples were divided into high and low Fescore groups, the corresponding survival analysis results were shown in Figure 7H. High Fescore group showed a significantly better prognosis of STS than low Fescore (p = 0.0025). Finally, a Sankey chart (Figure 7I) was drawn to summarize our above findings: Fe cluster A and gene cluster A were related to a better prognosis of STS and high Fescore while Fe cluster B and gene

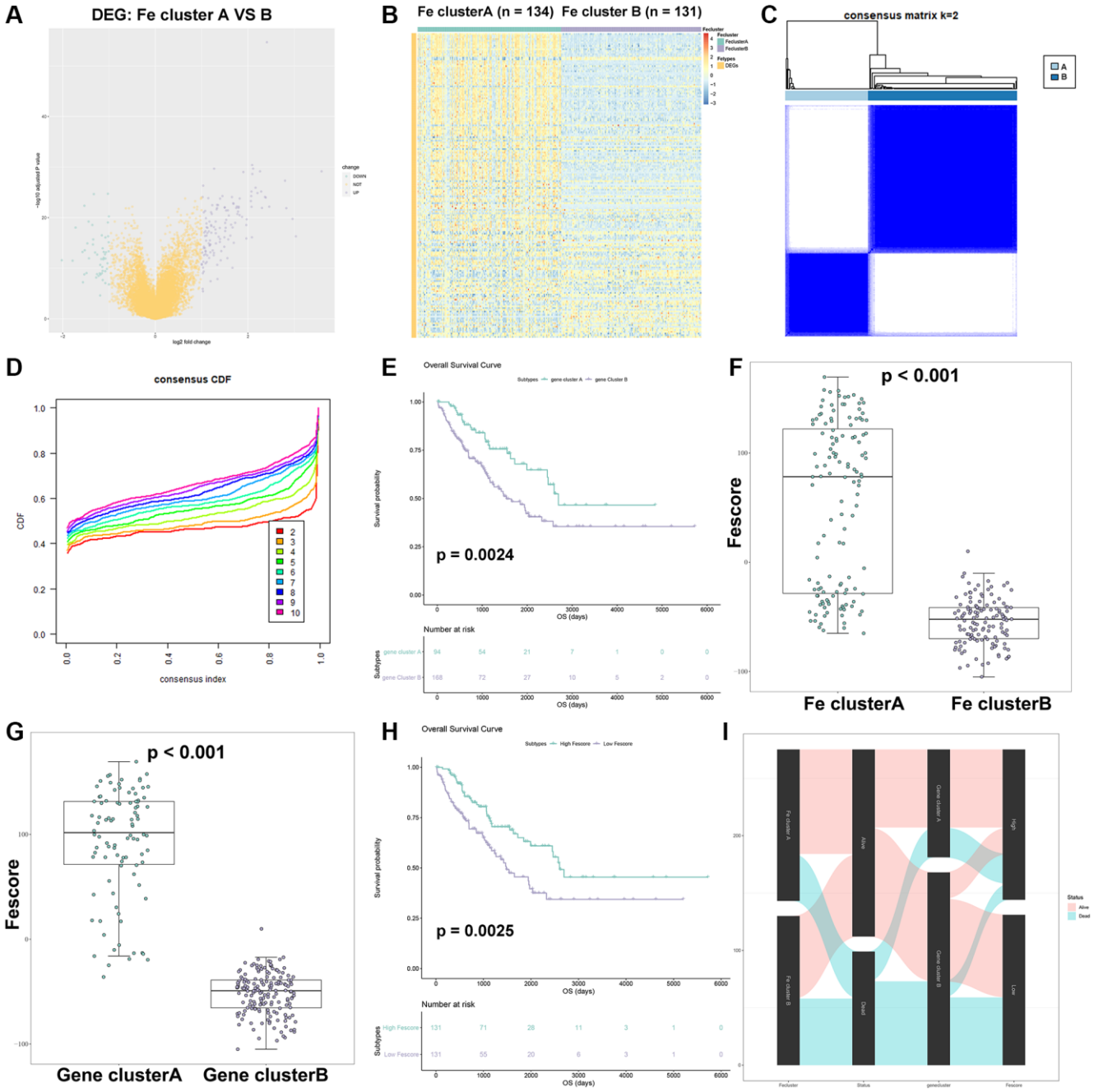

Figure 7. Construction of Fescore. (**A**) Volcano plot of DEGs between Fe cluster A and B. (**B**) The heatmap of expression of DEGs in Fe cluster A and B. (**C**) The result of consensus clustering analysis in STS based on 143 DEGs; The relationship between DEGs and these prognostic genes visualized as a Sankey diagram. (**D**) The cumulative distribution function plot in TCGA-SARC based on 143 DEGs. (**E**) Survival plot of gene clusters A and B in TCGA-SARC (p = 0.0024). (**F**) Comparison of Fescore among Fe clusters A and B. (**G**) Comparison of Fescore among gene clusters A and B. (**H**) Survival plot of high and low Fescore in TCGA-SARC (p = 0.0025). (**I**) The relationship between Fe clusters, gene clusters survival status and Fescore visualized as a Sankey diagram.

cluster B were related to a poorer outcome of STS and lower Fescore. The Fescore could quantify ferroptosis modification in STS and well indicate the clinical outcome of STS.

Fescore was related to the prognosis of multiple tumors

To further evaluate the prognostic value of Fescore in STS, the ROC curve of Fescore for predicting the survival of STS was shown in Figure 8A. Area under curve of Fescore predicting the 1 year, 3- and 5-years survival of STS were 0.85, 0.78, 0.75, respectively. Besides, a prognostic nomogram based on gender, age, race, metastasis, margin status and Fescore was also constructed (Figure 8B). The corresponding calibration curve of 1 year, 3- and 5-years survival of STS were also displayed in Figure 8C–8E. The nomogram could effectively predict the prognosis of STS. Besides, we further explored the prognostic value of Fescore in other

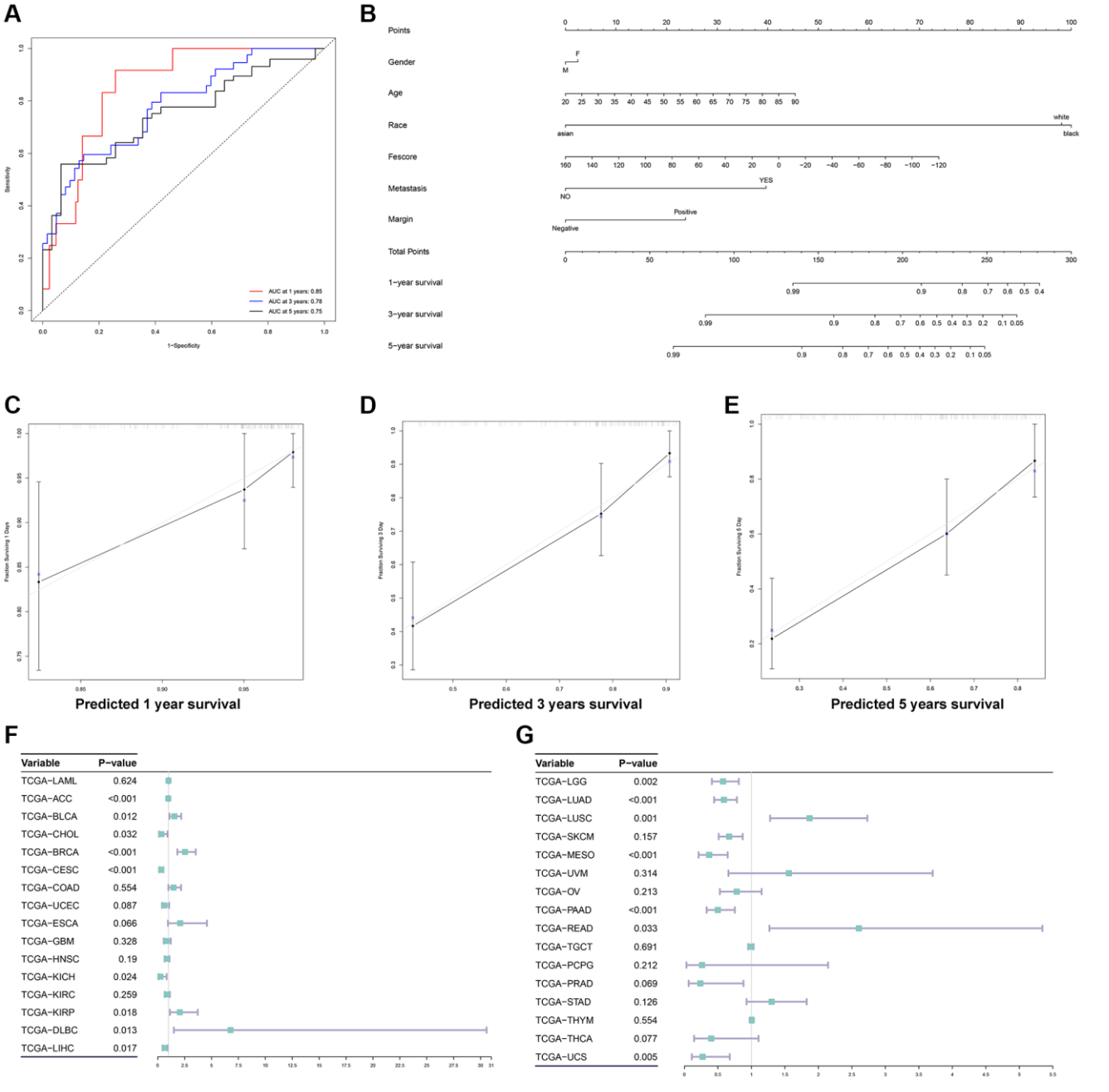

Figure 8. Construction of a prognostic nomogram and validation of the Fescore in multiple tumors. (**A**) ROC curve of Fescore for predicting the 1-year, 3- and 5-years survival of STS. (**B**) The prognostic nomogram based on gender, age, race, metastasis, margin status and Fescore for predicting the prognosis of STS. (**C–E**) The calibration curve of 1-year, 3- and 5-years survival of STS. (**F**, **G**) Validation of Fescore across 33 types of tumors.

32 tumors from TCGA database. The results of univariate Cox analysis of Fescore in different tumors were shown in Figure 8F, 8G. Among them, Fescore was significantly related to the prognosis of TCGA-ACC ($p < 0.001$), TCGA-BLCA ($p = 0.012$), TCGA-CHOL ($p = 0.032$), TCGA-BRCA ($p < 0.001$), TCGA-CESC ($p < 0.001$), TCGA-KICH ($p = 0.024$), TCGA-KIRP ($p = 0.018$), TCGA-DLBC ($p = 0.013$), TCGA-LIHC ($p = 0.017$), TCGA-LGG ($p = 0.002$), TCGA-LUAD ($p < 0.001$), TCGA-LUSC ($p = 0.001$), TCGA-MESO ($p < 0.001$), TCGA-PAAD ($p < 0.001$), TCGA-READ ($p = 0.033$) and TCGA-UCS ($p = 0.005$). We also tested the Fescore on different subtypes of STS including undifferentiated sarcoma, Liposarcoma, Leiomyosarcoma, Synovial Sarcoma, Ewing Sarcoma, and Fibrosis sarcoma through survival analysis, tumor grading, CINSARC index and metastasis analysis and results were shown in Supplementary Figure 8. While the significant differences between high and low Fescore groups were not detected in liposarcoma, Fescore could be applied to the majority of STS subtypes and well predicted its prognosis and clinical characteristics. The above results showed that the Fescore could serve as a prognostic predictor in a variety of tumors.

Fescore effectively predicted immunotherapy response

Next, we explored the role of Fescore in predicting tumor immunotherapy response. The Fescore was calculated for each sample in immunotherapy dataset IMvigor210 (PD-L1). Then survival curve among high and low Fescore groups was shown in Figure 9A. High Fescore group showed a better prognosis than low Fescore group ($p = 0.0027$). The relative percent of complete response (CR), Progressive disease (PD), partial response (PR) and stable disease (SD) in high Fescore group were 4.4%, 63.0%, 8.2% and 24.4%, respectively. Meanwhile in low Fescore group the relative percent of CR, PD, PR and SD were 2.0%, 75.8%, 8.1% and 14.1%, respectively. The relative percent of CR/PR in high Fescore group and low Fescore group were 12.6% and 10.1%, respectively (Figure 9B, 9C). These results indicated that high Fescore was correlated with a better immunotherapy outcome. The AUC of Fescore for predicting the immunotherapy response in IMvigor210 was 0.800 (Figure 9D).

Besides, the Fescore of each sample in immunotherapy dataset GSE78220 (PD-1) was also calculated. Compared with high Fescore group, low Fescore group exhibited a poorer prognosis (Figure 9E, $p = 0.17$). The relative percent of CR, PD, PR in high Fescore group were 25%, 40% and 35%, respectively. The proportion of PD and PR in low Fescore group were 62.5% and 37.5%, respectively. In high Fescore group CR/PR accounted for 60% while in low Fescore group CR/PR accounted for 37.5% (Figure 9F, 9G). The AUC of Fescore for predicting the immunotherapy response in GSE78220 was 0.750 (Figure 9H).

Moreover, the Fescore of samples from immunotherapy dataset GSE35640 (MAGE-A3) was calculated. In high Fescore group, 46.4% of the patients responded to immunotherapy while in low Fescore group this number dropped to 32.1% (Figure 9I). The AUC of Fescore for predicting the immunotherapy response in GSE35640 was 0.763 (Figure 9J). The above results show that Fescore had a good predictive effect in different immunotherapy response.

The downregulation of LOX inhibited the biological behavior of STS cells and increased the production of ROS

In order to further prove the robustness of Fescore, we performed experiments to verify the function of hub gene that constructed the Fescore in STS and its relationship with ferroptosis. First, we conducted protein-protein interaction analysis among the genes that constructed Fescore and further screened LOX as a hub gene based on degree more than 4 (Supplementary Figure 9). Then, we focused on whether LOX played an important role in ferroptosis. Then, the expression of LOX was knockdown in HT-1080 and A204 cells (Figure 10A, 10B). And EdU assay were used to evaluate the proliferative capacity of HT-1080 and A204 cells. When LOX was knocked down, the proliferation of HT-1080 and A204 cells were decreased (Figure 10C, 10D). Besides, ROS levels in HT-1080 and A204 cells were increased after LOX knockdown (Figure 10E, 10F). Furthermore, the HT-1080 and A204 cells migration were assessed by Transwell assay and the results showed that knockdown of LOX were inhibited the migration of HT-1080 and A2044 cells (Figure 10G, 10H).

DISCUSSION

Although STS is a rare tumor originated from mesenchymal tissue, there has been few breakthroughs to improve the prognosis of STS in recent decades. Ferroptosis, a special way of cell death, has been gradually found in a variety of cancer cells and promoting ferroptosis in tumor cells has become a novel treatment for cancer. For example, decreased KLF2 attenuated ferroptosis in renal cell carcinoma by regulating GPX4 level [40]. Induced ferroptosis in gastric cancer could also lead to the higher sensitivity of gastric cancer cells to cisplatin [41]. However, the role

and modification characteristics of ferroptosis in STS are still unclear. Therefore, it is urgent to clarify the classification of STS related to ferroptosis and quantify the modification of ferroptosis in STS.

In this study, we screened 16 ferroptosis regulators that were significantly related to the prognosis of STS, and further found that they showed great differences in both expression level and variation level. The functional enrichment analysis indicated differentially expressed ferroptosis regulators were enriched in cholesterol and glutathione biosynthetic processes and response to oxidative stress. A recent study revealed that glutathione biosynthesis and oxidative stress were closely related to the progression of ferroptosis [42]. In addition, previous research also reported that high cholesterol could make tumor cells resistant to ferroptosis, thus promoting tumor development [43]. Therefore, the differentially expressed ferroptosis regulators between normal and tumor tissues might also regulate ferroptosis through these pathways. SQLE, NFE2L2 and GSS were the ferroptosis regulators most related to the prognosis of STS. Further, the result of CNV implied that GSS and AIFM2 had the highest frequency of variation. A recent study showed that decreased expression of SQLE could lead to limited growth of liver cancer through p53 pathway [44]. Recent research indicated that reduced expression of NFE2L2 was related to a better prognosis of breast cancer [45]. In Chen's study GSS was also determined

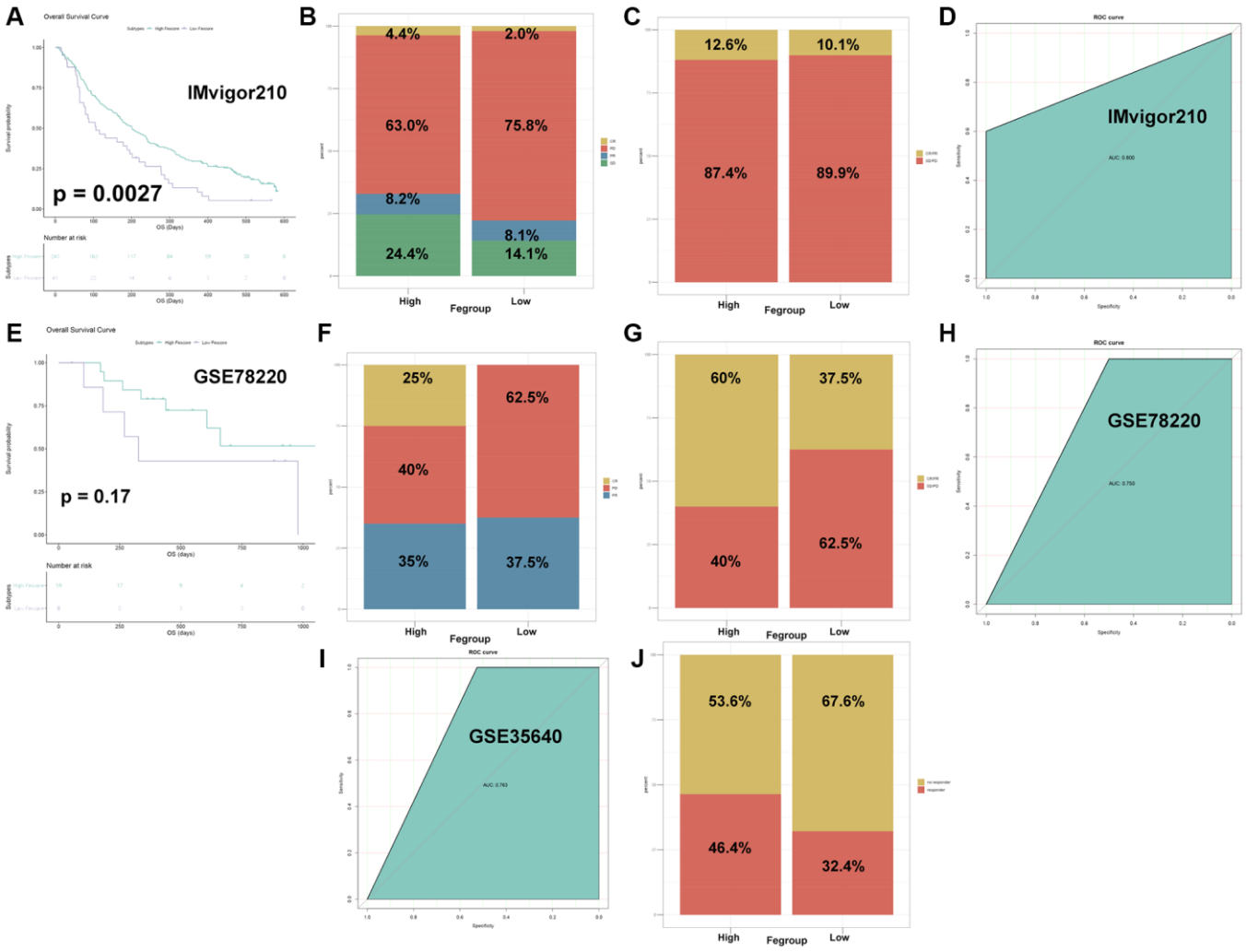

Figure 9. The Fescore predicted immune response in immunotherapy datasets. (**A**) Survival plot of high and low Fescore in IMvigor210 dataset (p = 0.0027). (**B**) Relative percent of immune responses in high and low Fescore in IMvigor210 dataset. Abbreviations: CR: complete response; PR: partial response; SD: stable disease; PD: progressive disease. (**C**) Relative percent of CR/PR and SD/PD in high and low Fescore in IMvigor210 dataset. (**D**) ROC curve for prediction of immune response in IMvigor210 dataset. (**E**) Survival plot of high and low Fescore in GSE78220 dataset (p = 0.17). (**F**) Relative percent of immune responses in high and low Fescore in GSE78220 dataset. Abbreviations: CR: complete response; PR: partial response; PD: progressive disease. (**G**) Relative percent of CR/PR and SD/PD in high and low Fescore in GSE78220 dataset. (**H**) ROC curve for prediction of immune response in GSE78220 dataset. (**I**) ROC curve for prediction of immune response in GSE35640 dataset. (**J**) Relative percent of CR/PR and SD/PD in high and low Fescore in GSE35640 dataset.

as a potential target against tumor by regulating polydatin [46]. Increased GSS was also found to enhance the resistance to cisplatin in ovarian cancer [47]. Activated AIFM2 could also accelerate the apoptosis in lung cancer [48]. These literature reports were consistent with our analysis, which also suggested that these ferroptosis regulators might be important for STS progression.

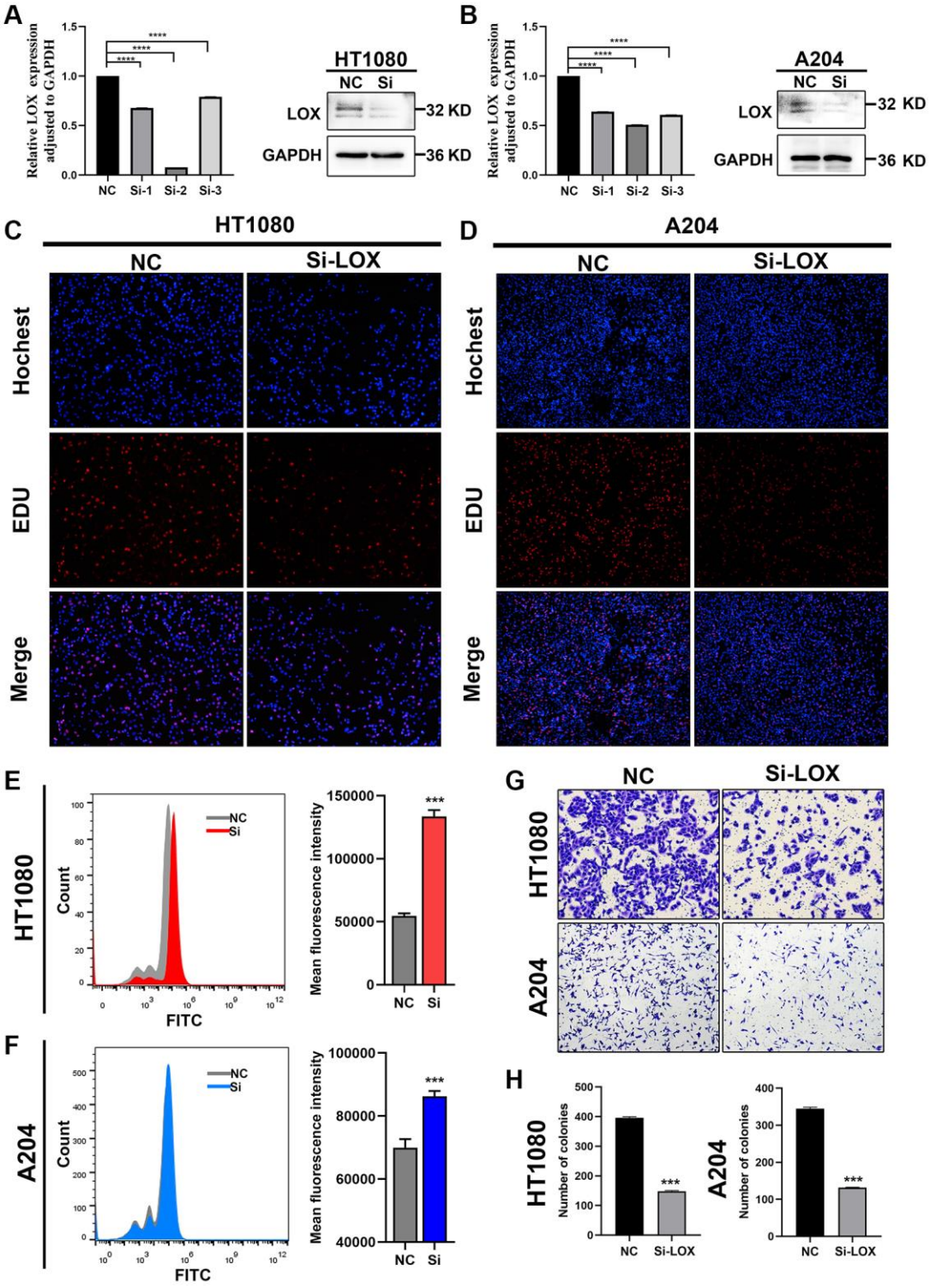

Figure 10. Downregulation of LOX inhibits growth and increases ROS production in HT1080 and A204 cells. (**A**, **B**) qPCR analysis and Western blotting analysis were performed to detect the mRNA and protein levels of LOX in HT-1080 and A204 cells. (**C**, **D**) EdU assay was used to detect the proliferation of HT-1080 and A204 cells. (**E**, **F**) ROS levels were analyzed by flow cytometry in HT-1080 and A204 cells. (**G**, **H**) Transwell assay was performed to assess migration of HT-1080 and A204 cells. $^{***}p < 0.001$, $^{****}p = 0$.

By using consensus clustering, we identified two different ferroptosis modification patterns in STS. These two Fe clusters showed significant differences in prognosis and enrichment pathways. Fe cluster A was correlated with p53 pathway and had a better prognosis of STS while Fe cluster B was correlated with angiogenesis and MYC pathway and showed a poorer outcome of STS. P53 pathway is a recognized pathway that inhibit tumor progression [49]. Angiogenesis has also been proven to be a key part of tumor progression. A recent study reported that angiogenesis was necessary for bladder cancer progression [50]. MYC is an oncogene accelerating tumor progression. A latest study revealed that MYC could inhibit tumor immunity in neuroblastoma and melanoma [51]. The immune infiltration among different ferroptosis modification revealed that M2 macrophage was enriched in Fe cluster B while CD8 T cell was enriched in Fe cluster A. M2 macrophages have been proved to promote tumor development in many studies. A recent study implied that M2 macrophage polarization induced by FNDC5 was associated with hepatocellular carcinoma cell growth [52]. A former study also reported that M2 macrophage was related to poor prognosis of lung cancer [53]. These reports supported our results and indicated that different ferroptosis modification patterns were correlated with the prognosis and immune infiltration of STS.

The cMap analysis screened sulfadimethoxine and withaferin A based on different ferroptosis modification patterns. A former study reported that sulfadimethoxine could be used as potential drugs against breast cancer and colon cancer [54]. Withaferin A, a promising compound with anti-tumor potential, has been studied in many fields. A recent article showed that withaferin A could be a potential target treating breast cancer [55]. Moreover, withaferin A could also promote apoptosis in osteosarcoma cell [56]. These drugs might be potential targets against STS. The Fe clusters and gene clusters determined based on DEGs had a great intersection with each other, indicating the consensus clustering was relatively stable. Besides, high Fescore group showed a significantly better prognosis of STS than low Fescore. The prognostic nomogram also effectively predicted the survival of STS and the ROC curve of Fescore for predicting the prognosis of STS showed that Fescore was a good prognostic predictor. Fescore was also significant correlated with the prognosis of 16 other tumors from TCGA. Fescore played a protective role in some tumors while in other tumors, Fescore was a risk factor, which might be due to the heterogeneity between different tumors.

Tumor immunotherapy has been controversial because of its limited application and high price. Therefore, exploring a good predictor to predict the outcome and prognosis of tumor immunotherapy is of great significance. Here we reported the Fescore could well predict the immunotherapeutic response in different kinds of immunotherapy (MAGE-A3, PD-1/L1). High Fescore also was correlated with better immunotherapeutic response and prognosis. Hence, the Fescore could also be used to predict the response to tumor immunotherapy, which contribute to the clinical application of tumor immunotherapy in the future.

Our further experiments also showed that LOX, as the hub gene in Fescore, could regulate the STS progression. Iron is involved in the activation of LOX, an iron-containing enzyme that promotes the generation of lipid ROS such as lipid peroxides [57]. Increased lipid peroxidation subsequently leads to damage and rupture of cellular and mitochondrial membranes, causing ferroptosis. EDU proliferation experiments and Transwell experiments confirmed that LOX had an important value in STS. The ROS experiment showed that LOX played a role through ferroptosis and affected the prognosis of tumors, which was also consistent with Shintoku's reports [57].

Although we determined different modifications of ferroptosis in STS and established the Fescore to quantify the modification of ferroptosis, our study still had limitations. First of all, the modifications of ferroptosis in STS were identified by public datasets, and more clinical samples were needed to perform transcriptome sequencing to validate the Fescore. Secondly, we also noticed that due to different sequencing methods, population baselines (race, gender, stage, etc.), and sampling methods, there was some heterogeneity among datasets. Although the Fescore could well predict the prognosis and immunotherapy response in different cohorts, larger STS cohorts are needed for further research. Thirdly, due to the difference of subtypes of STS, few immune cells had different infiltration between the ferroptosis modification patterns. We are currently collecting clinical STS samples from our department and will continue to conduct ferroptosis-related research. We also hope more researchers will pay attention to this field.

CONCLUSION

In summary, we identified different modifications of ferroptosis in STS and constructed the Fescore to quantify the modification of ferroptosis. The Fescore was significantly related to the immune infiltration and prognosis of STS and immunotherapy response. The Fescore was also successfully validated in multiple tumors and STS subtypes. Therefore, the Fescore could provide a new prospect for precision medicine and tumor immunotherapy.

Abbreviations

STS: Soft tissue sarcoma; CNV: Copy number variation; PCA: Principal component analysis; GSEA: Gene set enrichment analysis; TCGA: The Cancer Genome Atlas; GEO: Gene Expression Omnibus; FPKM: Fragments Per Kilobase Million; DEGs: Differentially expressed genes; cMap: Connectivity map; HR: Hazard ratio; ROC: Receiver operating characteristic; GEO: Gene expression omnibus; TME: Tumor microenvironment; ES: Enrichment score; AUC: Area under curve; GO: Gene ontology; FDR: False discovery rate; ROS: Reactive oxygen species.

AUTHOR CONTRIBUTIONS

L.C., Z.-Q.Y., L.-Y.G. and M.-H.W. conceived and designed the study. C.Z., M.-H.W. and F.-F.Y. searched databases and analyzed data. Z.-Q.Y. and K.-W.X. prepared Supplementary Tables 1–11, Figures 1–10 and Supplementary Figures 1–9. L.C. and Z.-Q.Y. wrote the manuscript. L.C. and F.-F.Y. supervised the study. Z. Q.Y., L.-Y.G., K.-W.X., M.-H.W. and C.Z. performed the experiments. All authors made substantial contributions to conception and design of this study. All authors reviewed the manuscript.

CONFLICTS OF INTEREST

The authors declare no conflicts of interest related to this study.

ETHICAL STATEMENT AND CONSENT

This study was approved by the Institutional Ethics board of Zhongnan Hospital of Wuhan University. The informed consents were obtained from all patients (Ethical batch No.: 2021150).

FUNDING

This work was supported by the Health Care of Yellow Crane Talent Plan (Project No. 17).

REFERENCES

1. Brennan MF. Soft tissue sarcoma: advances in understanding and management. Surgeon. 2005; 3:216–23. https://doi.org/10.1016/s1479-666x(05)80044-7 PMID:16076008

2. Siegel RL, Miller KD, Fuchs HE, Jemal A. Cancer Statistics, 2021. CA Cancer J Clin. 2021; 71:7–33. https://doi.org/10.3322/caac.21654 PMID:33433946

3. Prosnitz LR, Maguire P, Anderson JM, Scully SP, Harrelson JM, Jones EL, Dewhirst M, Samulski TV, Powers BE, Rosner GL, Dodge RK, Layfield L, Clough R, Brizel DM. The treatment of high-grade soft tissue sarcomas with preoperative thermoradiotherapy. Int J Radiat Oncol Biol Phys. 1999; 45:941–9. https://doi.org/10.1016/s0360-3016(99)00272-2 PMID:10571201

4. Tawbi HA, Burgess M, Bolejack V, Van Tine BA, Schuetze SM, Hu J, D'Angelo S, Attia S, Riedel RF, Priebat DA, Movva S, Davis LE, Okuno SH, et al. Pembrolizumab in advanced soft-tissue sarcoma and bone sarcoma (SARC028): a multicentre, two-cohort, single-arm, open-label, phase 2 trial. Lancet Oncol. 2017; 18:1493–501. https://doi.org/10.1016/S1470-2045(17)30624-1 PMID:28988646

5. Dixon SJ, Lemberg KM, Lamprecht MR, Skouta R, Zaitsev EM, Gleason CE, Patel DN, Bauer AJ, Cantley AM, Yang WS, Morrison B 3rd, Stockwell BR. Ferroptosis: an iron-dependent form of nonapoptotic cell death. Cell. 2012; 149:1060–72. https://doi.org/10.1016/j.cell.2012.03.042 PMID:22632970

6. Kauffman ME, Kauffman MK, Traore K, Zhu H, Trush MA, Jia Z, Li YR. MitoSOX-Based Flow Cytometry for Detecting Mitochondrial ROS. React Oxyg Species (Apex). 2016; 2:361–70. https://doi.org/10.20455/ros.2016.865 PMID:29721549

7. Dächert J, Ehrenfeld V, Habermann K, Dolgikh N, Fulda S. Targeting ferroptosis in rhabdomyosarcoma cells. Int J Cancer. 2020; 146:510–20. https://doi.org/10.1002/ijc.32496 PMID:31173656

8. Brashears CB, Prudner BC, Rathore R, Caldwell KE, Dehner CA, Buchanan JL, Lange SES, Poulin N, Sehn JK, Roszik J, Spitzer D, Jones KB, O'Keefe R, et al. Malic Enzyme 1 Absence in Synovial Sarcoma Shifts Antioxidant System Dependence and Increases Sensitivity to Ferroptosis Induction with ACXT-3102. Clin Cancer Res. 2022; 28:3573–89. https://doi.org/10.1158/1078-0432.CCR-22-0470 PMID:35421237

9. Schut AW, Vriends ALM, Sacchetti A, Timbergen MJM, Alman BA, Al-Jazrawe M, Grünhagen DJ, Verhoef C, Sleijfer S, Wiemer EAC. In desmoid-type fibromatosis cells sorafenib induces ferroptosis and apoptosis, which are enhanced by autophagy inhibition. Eur J Surg Oncol. 2022; 48:1527–35. https://doi.org/10.1016/j.ejso.2022.02.020 PMID:35221159

10. Pardoll DM. The blockade of immune checkpoints in cancer immunotherapy. Nat Rev Cancer. 2012; 12:252–64. https://doi.org/10.1038/nrc3239 PMID:22437870

11. Topalian SL, Hodi FS, Brahmer JR, Gettinger SN, Smith DC, McDermott DF, Powderly JD, Carvajal RD, Sosman JA, Atkins MB, Leming PD, Spigel DR, Antonia SJ, et al. Safety, activity, and immune correlates of anti-PD-1 antibody in cancer. N Engl J Med. 2012; 366:2443–54. https://doi.org/10.1056/NEJMoa1200690 PMID:22658127

12. Eppihimer MJ, Gunn J, Freeman GJ, Greenfield EA, Chernova T, Erickson J, Leonard JP. Expression and regulation of the PD-L1 immunoinhibitory molecule on microvascular endothelial cells. Microcirculation. 2002; 9:133–45. https://doi.org/10.1038/sj/mn/7800123 PMID:11932780

13. Wang X, Yang L, Huang F, Zhang Q, Liu S, Ma L, You Z. Inflammatory cytokines IL-17 and TNF-α up-regulate PD-L1 expression in human prostate and colon cancer cells. Immunol Lett. 2017; 184:7–14. https://doi.org/10.1016/j.imlet.2017.02.006 PMID:28223102

14. Song S, Yuan P, Wu H, Chen J, Fu J, Li P, Lu J, Wei W. Dendritic cells with an increased PD-L1 by TGF-β induce T cell anergy for the cytotoxicity of hepatocellular carcinoma cells. Int Immunopharmacol. 2014; 20:117–23. https://doi.org/10.1016/j.intimp.2014.02.027 PMID:24606770

15. Xiao KW, Yang ZQ, Yan X, Liu ZB, Yang M, Guo LY, Cai L. Molecular Characteristics of m6A Regulators and Tumor Microenvironment Infiltration in Soft Tissue Sarcoma: A Gene-Based Study. Front Bioeng Biotechnol. 2022; 10:846812. https://doi.org/10.3389/fbioe.2022.846812 PMID:35519620

16. Wilkerson MD, Hayes DN. ConsensusClusterPlus: a class discovery tool with confidence assessments and item tracking. Bioinformatics. 2010; 26:1572–3. https://doi.org/10.1093/bioinformatics/btq170 PMID:20427518

17. Chen B, Khodadoust MS, Liu CL, Newman AM, Alizadeh AA. Profiling Tumor Infiltrating Immune Cells with CIBERSORT. Methods Mol Biol. 2018; 1711:243–59. https://doi.org/10.1007/978-1-4939-7493-1_12 PMID:29344893

18. Savola S, Klami A, Myllykangas S, Manara C, Scotlandi K, Picci P, Knuutila S, Vakkila J. High Expression of Complement Component 5 (C5) at Tumor Site Associates with Superior Survival in Ewing's Sarcoma Family of Tumour Patients. ISRN Oncol. 2011; 2011:168712. https://doi.org/10.5402/2011/168712 PMID:22084725

19. Gultekin O, Gonzalez-Molina J, Hardell E, Moyano-Galceran L, Mitsios N, Mulder J, Kokaraki G, Isaksson A, Sarhan D, Lehti K, Carlson JW. FOXP3+ T cells in uterine sarcomas are associated with favorable prognosis, low extracellular matrix expression and reduced YAP activation. NPJ Precis Oncol. 2021; 5:97. https://doi.org/10.1038/s41698-021-00236-6 PMID:34799669

20. Darbo E, Pérot G, Darmusey L, Le Guellec S, Leroy L, Gaston L, Desplat N, Thébault N, Merle C, Rochaix P, Valentin T, Ferron G, Chevreau C, et al. Distinct Cellular Origins and Differentiation Process Account for Distinct Oncogenic and Clinical Behaviors of Leiomyosarcomas. Cancers (Basel). 2023; 15:534. https://doi.org/10.3390/cancers15020534 PMID:36672483

21. Lagarde P, Przybyl J, Brulard C, Pérot G, Pierron G, Delattre O, Sciot R, Wozniak A, Schöffski P, Terrier P, Neuville A, Coindre JM, Italiano A, et al. Chromosome instability accounts for reverse metastatic outcomes of pediatric and adult synovial sarcomas. J Clin Oncol. 2013; 31:608–15. https://doi.org/10.1200/JCO.2012.46.0147 PMID:23319690

22. Darmusey L, Pérot G, Thébault N, Le Guellec S, Desplat N, Gaston L, Delespaul L, Lesluyes T, Darbo E, Gomez-Brouchet A, Richard E, Baud J, Leroy L, et al. ATRX Alteration Contributes to Tumor Growth and Immune Escape in Pleomorphic Sarcomas. Cancers (Basel). 2021; 13:2151. https://doi.org/10.3390/cancers13092151 PMID:33946962

23. Liang JY, Wang DS, Lin HC, Chen XX, Yang H, Zheng Y, Li YH. A Novel Ferroptosis-related Gene Signature for Overall Survival Prediction in Patients with Hepatocellular Carcinoma. Int J Biol Sci. 2020; 16:2430–41. https://doi.org/10.7150/ijbs.45050 PMID:32760210

24. Zuo YH, Han QB, Dong GT, Yue RQ, Ren XC, Liu JX, Liu L, Luo P, Zhou H. *Panax ginseng* Polysaccharide Protected H9c2 Cardiomyocyte From Hypoxia/Reoxygenation Injury Through Regulating Mitochondrial Metabolism and RISK Pathway. Front Physiol. 2018; 9:699. https://doi.org/10.3389/fphys.2018.00699 PMID:29962955

25. Heagerty PJ, Lumley T, Pepe MS. Time-dependent ROC curves for censored survival data and a diagnostic marker. Biometrics. 2000; 56:337–44.

https://doi.org/10.1111/j.0006-341x.2000.00337.x
PMID:10877287

26. Ritchie ME, Phipson B, Wu D, Hu Y, Law CW, Shi W, Smyth GK. limma powers differential expression analyses for RNA-sequencing and microarray studies. Nucleic Acids Res. 2015; 43:e47. https://doi.org/10.1093/nar/gkv007 PMID:25605792

27. Storey JD. A Direct Approach to False Discovery Rates. J R Stat Soc Series B Stat Methodol. 2002; 64:479–98. https://doi.org/10.1111/1467-9868.00346

28. Lamb J, Crawford ED, Peck D, Modell JW, Blat IC, Wrobel MJ, Lerner J, Brunet JP, Subramanian A, Ross KN, Reich M, Hieronymus H, Wei G, et al. The Connectivity Map: using gene-expression signatures to connect small molecules, genes, and disease. Science. 2006; 313:1929–35. https://doi.org/10.1126/science.1132939 PMID:17008526

29. Yoshihara K, Shahmoradgoli M, Martínez E, Vegesna R, Kim H, Torres-Garcia W, Treviño V, Shen H, Laird PW, Levine DA, Carter SL, Getz G, Stemke-Hale K, et al. Inferring tumour purity and stromal and immune cell admixture from expression data. Nat Commun. 2013; 4:2612. https://doi.org/10.1038/ncomms3612 PMID:24113773

30. Yu G, Wang LG, Han Y, He QY. clusterProfiler: an R package for comparing biological themes among gene clusters. OMICS. 2012; 16:284–7. https://doi.org/10.1089/omi.2011.0118 PMID:22455463

31. Subramanian A, Tamayo P, Mootha VK, Mukherjee S, Ebert BL, Gillette MA, Paulovich A, Pomeroy SL, Golub TR, Lander ES, Mesirov JP. Gene set enrichment analysis: a knowledge-based approach for interpreting genome-wide expression profiles. Proc Natl Acad Sci U S A. 2005; 102:15545–50. https://doi.org/10.1073/pnas.0506580102 PMID:16199517

32. Sotiriou C, Wirapati P, Loi S, Harris A, Fox S, Smeds J, Nordgren H, Farmer P, Praz V, Haibe-Kains B, Desmedt C, Larsimont D, Cardoso F, et al. Gene expression profiling in breast cancer: understanding the molecular basis of histologic grade to improve prognosis. J Natl Cancer Inst. 2006; 98:262–72. https://doi.org/10.1093/jnci/djj052 PMID:16478745

33. Mayakonda A, Lin DC, Assenov Y, Plass C, Koeffler HP. Maftools: efficient and comprehensive analysis of somatic variants in cancer. Genome Res. 2018; 28:1747–56. https://doi.org/10.1101/gr.239244.118 PMID:30341162

34. Krzywinski M, Schein J, Birol I, Connors J, Gascoyne R, Horsman D, Jones SJ, Marra MA. Circos: an information aesthetic for comparative genomics. Genome Res. 2009; 19:1639–45. https://doi.org/10.1101/gr.092759.109 PMID:19541911

35. Friendly M. Corrgrams: Exploratory Displays for Correlation Matrices. Am Stat. 2002; 56:316–24. https://doi.org/10.1198/000313002533

36. Harrell FE Jr, Lee KL, Mark DB. Multivariable prognostic models: issues in developing models, evaluating assumptions and adequacy, and measuring and reducing errors. Statist Med. 1996; 15:361–87. https://doi.org/10.1002/(SICI)1097-0258(19960229)15:4<361::AID-SIM168>3.0.CO;2-4

37. Wang L, Cao C, Ma Q, Zeng Q, Wang H, Cheng Z, Zhu G, Qi J, Ma H, Nian H, Wang Y. RNA-seq analyses of multiple meristems of soybean: novel and alternative transcripts, evolutionary and functional implications. BMC Plant Biol. 2014; 14:169. https://doi.org/10.1186/1471-2229-14-169 PMID:24939556

38. Lê S, Josse J, Husson F. FactoMineR: An R Package for Multivariate Analysis. J Stat Soft. 2008; 25:1–18. https://doi.org/10.18637/jss.v025.i01

39. Lopes CT, Franz M, Kazi F, Donaldson SL, Morris Q, Bader GD. Cytoscape Web: an interactive web-based network browser. Bioinformatics. 2010; 26:2347–8. https://doi.org/10.1093/bioinformatics/btq430 PMID:20656902

40. Lu Y, Qin H, Jiang B, Lu W, Hao J, Cao W, Du L, Chen W, Zhao X, Guo H. KLF2 inhibits cancer cell migration and invasion by regulating ferroptosis through GPX4 in clear cell renal cell carcinoma. Cancer Lett. 2021; 522:1–13. https://doi.org/10.1016/j.canlet.2021.09.014 PMID:34520818

41. Fu D, Wang C, Yu L, Yu R. Induction of ferroptosis by ATF3 elevation alleviates cisplatin resistance in gastric cancer by restraining Nrf2/Keap1/xCT signaling. Cell Mol Biol Lett. 2021; 26:26. https://doi.org/10.1186/s11658-021-00271-y PMID:34098867

42. Hayashima K, Katoh H. Expression of gamma-glutamyltransferase 1 in glioblastoma cells confers resistance to cystine deprivation-induced ferroptosis. J Biol Chem. 2022; 298:101703. https://doi.org/10.1016/j.jbc.2022.101703 PMID:35148992

43. Liu W, Chakraborty B, Safi R, Kazmin D, Chang CY, McDonnell DP. Dysregulated cholesterol homeostasis results in resistance to ferroptosis increasing tumorigenicity and metastasis in cancer. Nat Commun. 2021; 12:5103. https://doi.org/10.1038/s41467-021-25354-4 PMID:34429409

44. Sun H, Li L, Li W, Yang F, Zhang Z, Liu Z, Du W. p53 transcriptionally regulates SQLE to repress cholesterol synthesis and tumor growth. EMBO Rep. 2021; 22:e52537. https://doi.org/10.15252/embr.202152537 PMID:34459531

45. Wolf B, Goebel G, Hackl H, Fiegl H. Reduced mRNA expression levels of NFE2L2 are associated with poor outcome in breast cancer patients. BMC Cancer. 2016; 16:821. https://doi.org/10.1186/s12885-016-2840-x PMID:27770790

46. Chen P, Wang L, Sun S, Zhou Q, Zeng Z, Hu M, Hussain M, Lu C, Du H. High-throughput screening suggests glutathione synthetase as an anti-tumor target of polydatin using human proteome chip. Int J Biol Macromol. 2020; 161:1230–9. https://doi.org/10.1016/j.ijbiomac.2020.06.061 PMID:32544581

47. Godwin AK, Meister A, O'Dwyer PJ, Huang CS, Hamilton TC, Anderson ME. High resistance to cisplatin in human ovarian cancer cell lines is associated with marked increase of glutathione synthesis. Proc Natl Acad Sci U S A. 1992; 89:3070–4. https://doi.org/10.1073/pnas.89.7.3070 PMID:1348364

48. Lu J, Chen J, Xu N, Wu J, Kang Y, Shen T, Kong H, Ma C, Cheng M, Shao Z, Xu L, Zhao X. Activation of AIFM2 enhances apoptosis of human lung cancer cells undergoing toxicological stress. Toxicol Lett. 2016; 258:227–36. https://doi.org/10.1016/j.toxlet.2016.07.002 PMID:27392435

49. Levine AJ. p53, the cellular gatekeeper for growth and division. Cell. 1997; 88:323–31. https://doi.org/10.1016/s0092-8674(00)81871-1 PMID:9039259

50. Li X, Wei Z, Yu H, Xu Y, He W, Zhou X, Gou X. Secretory autophagy-induced bladder tumour-derived extracellular vesicle secretion promotes angiogenesis by activating the TPX2-mediated phosphorylation of the AURKA-PI3K-AKT axis. Cancer Lett. 2021; 523:10–28. https://doi.org/10.1016/j.canlet.2021.09.036 PMID:34597712

51. Wu X, Nelson M, Basu M, Srinivasan P, Lazarski C, Zhang P, Zheng P, Sandler AD. MYC oncogene is associated with suppression of tumor immunity and targeting Myc induces tumor cell immunogenicity for therapeutic whole cell vaccination. J Immunother Cancer. 2021; 9:e001388. https://doi.org/10.1136/jitc-2020-001388 PMID:33757986

52. Liu H, Wang M, Jin Z, Sun D, Zhu T, Liu X, Tan X, Shi G. FNDC5 induces M2 macrophage polarization and promotes hepatocellular carcinoma cell growth by affecting the PPARγ/NF-κB/NLRP3 pathway. Biochem Biophys Res Commun. 2021; 582:77–85. https://doi.org/10.1016/j.bbrc.2021.10.041 PMID:34695754

53. Xu F, Cui WQ, Wei Y, Cui J, Qiu J, Hu LL, Gong WY, Dong JC, Liu BJ. Astragaloside IV inhibits lung cancer progression and metastasis by modulating macrophage polarization through AMPK signaling. J Exp Clin Cancer Res. 2018; 37:207. https://doi.org/10.1186/s13046-018-0878-0 PMID:30157903

54. Di Pilato M, Kfuri-Rubens R, Pruessmann JN, Ozga AJ, Messemaker M, Cadilha BL, Sivakumar R, Cianciaruso C, Warner RD, Marangoni F, Carrizosa E, Lesch S, Billingsley J, et al. CXCR6 positions cytotoxic T cells to receive critical survival signals in the tumor microenvironment. Cell. 2021; 184:4512–30.e22. https://doi.org/10.1016/j.cell.2021.07.015 PMID:34343496

55. Ambrose JM, Veeraraghavan VP, Kullappan M, Velmurugan D, Vennila R, Rupert S, Dorairaj S, Surapaneni KM. Molecular modeling studies of the effects of withaferin A and its derivatives against oncoproteins associated with breast cancer stem cell activity. Process Biochem. 2021; 111:186–99. https://doi.org/10.1016/j.procbio.2021.09.007

56. Zhang HL, Zhang H. Withaferin-A Induces Apoptosis in Osteosarcoma U2OS Cell Line via Generation of ROS and Disruption of Mitochondrial Membrane Potential. Pharmacogn Mag. 2017; 13:523–7. https://doi.org/10.4103/0973-1296.211042 PMID:28839383

57. Shintoku R, Takigawa Y, Yamada K, Kubota C, Yoshimoto Y, Takeuchi T, Koshiishi I, Torii S. Lipoxygenase-mediated generation of lipid peroxides enhances ferroptosis induced by erastin and RSL3. Cancer Sci. 2017; 108:2187–94. https://doi.org/10.1111/cas.13380 PMID:28837253

SUPPLEMENTARY MATERIALS

Supplementary Figures

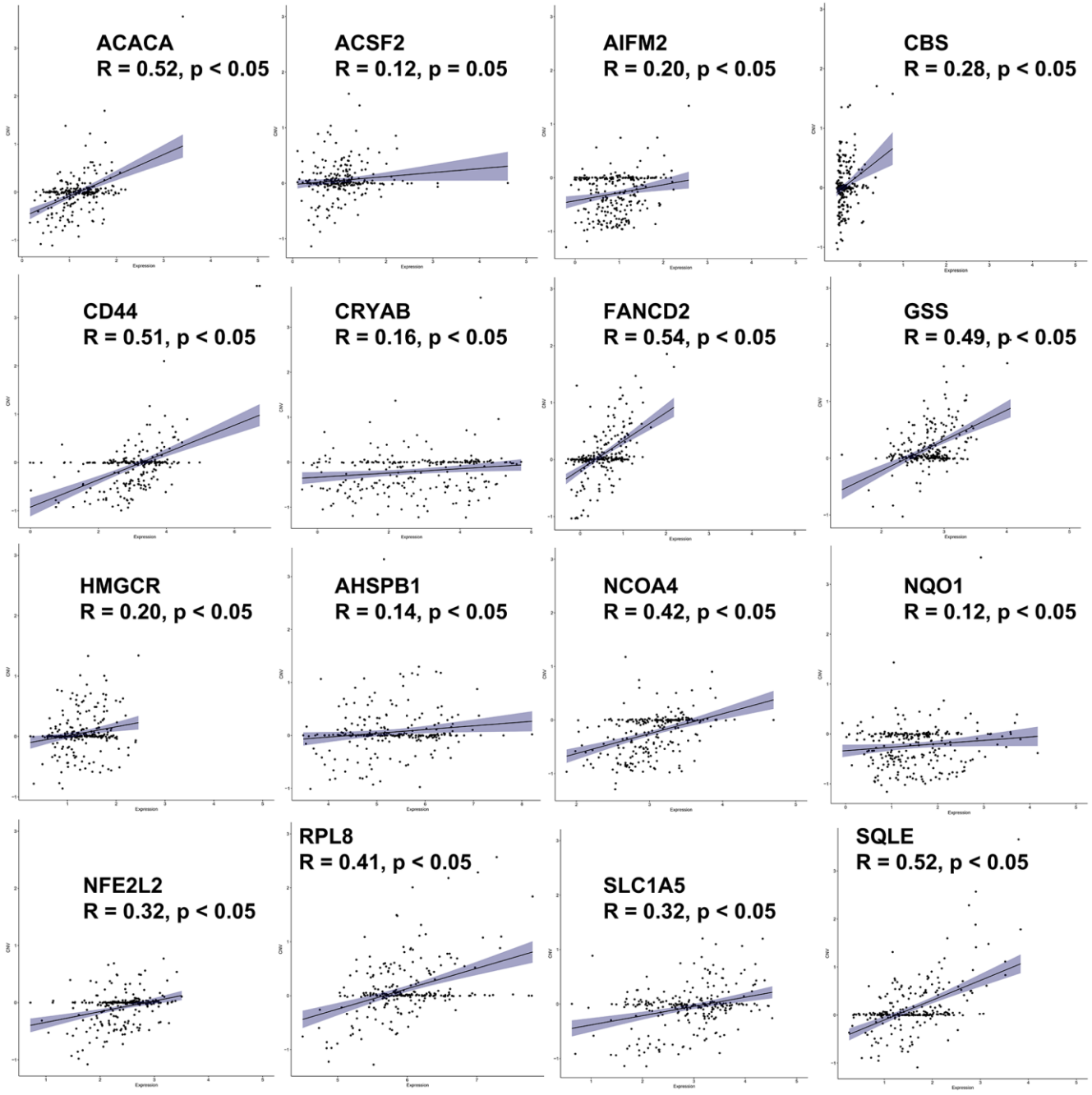

Supplementary Figure 1. The relationship between CNV and expression of ferroptosis regulators.

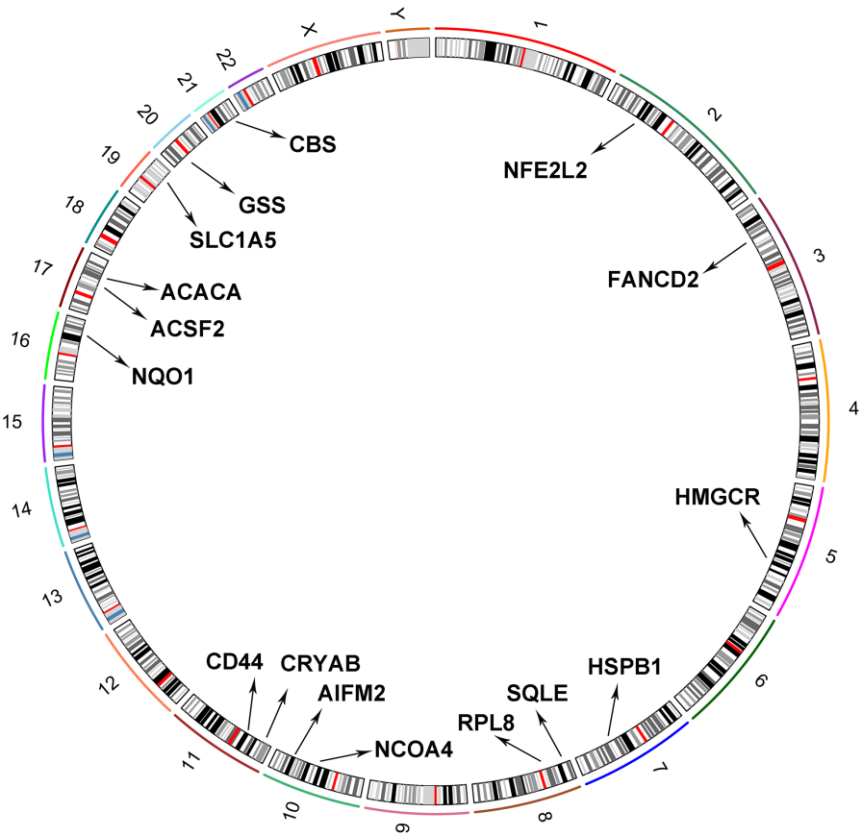

Supplementary Figure 2. The relative location of 16 ferroptosis regulators.

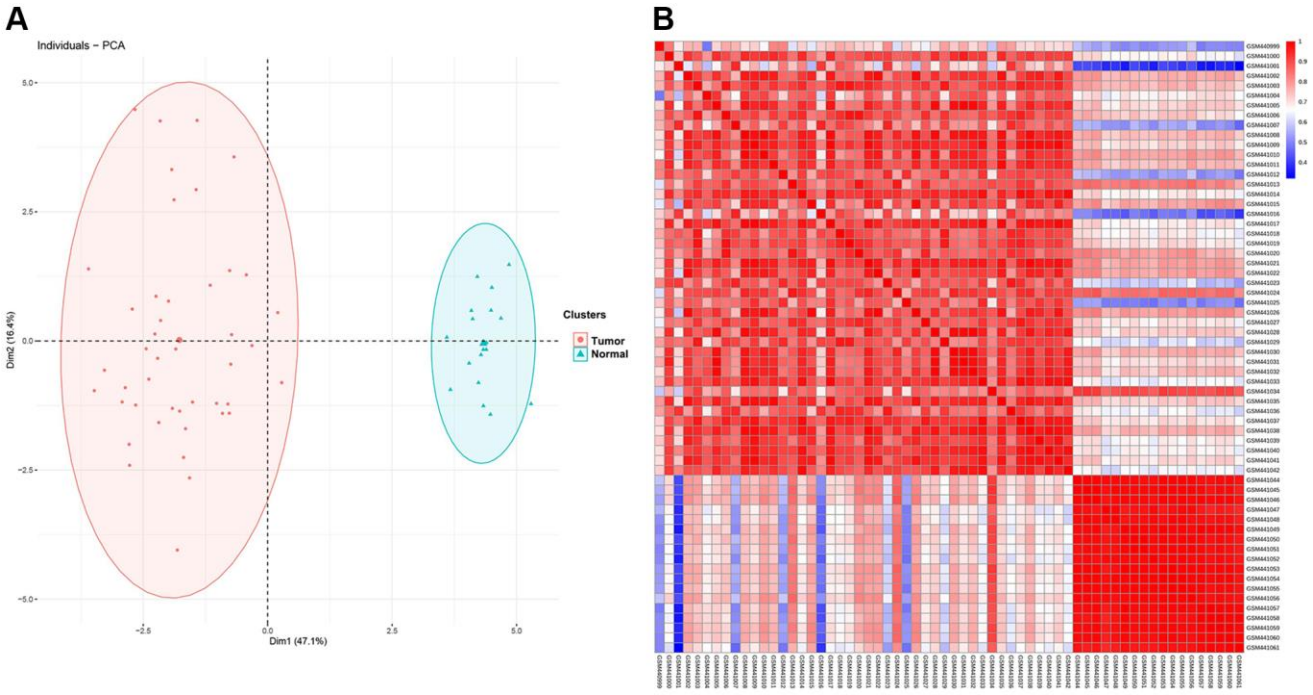

Supplementary Figure 3. The PCA (**A**) and sample correlation heatmaps (**B**) of normal and tumor samples based on expression of ferroptosis regulators.

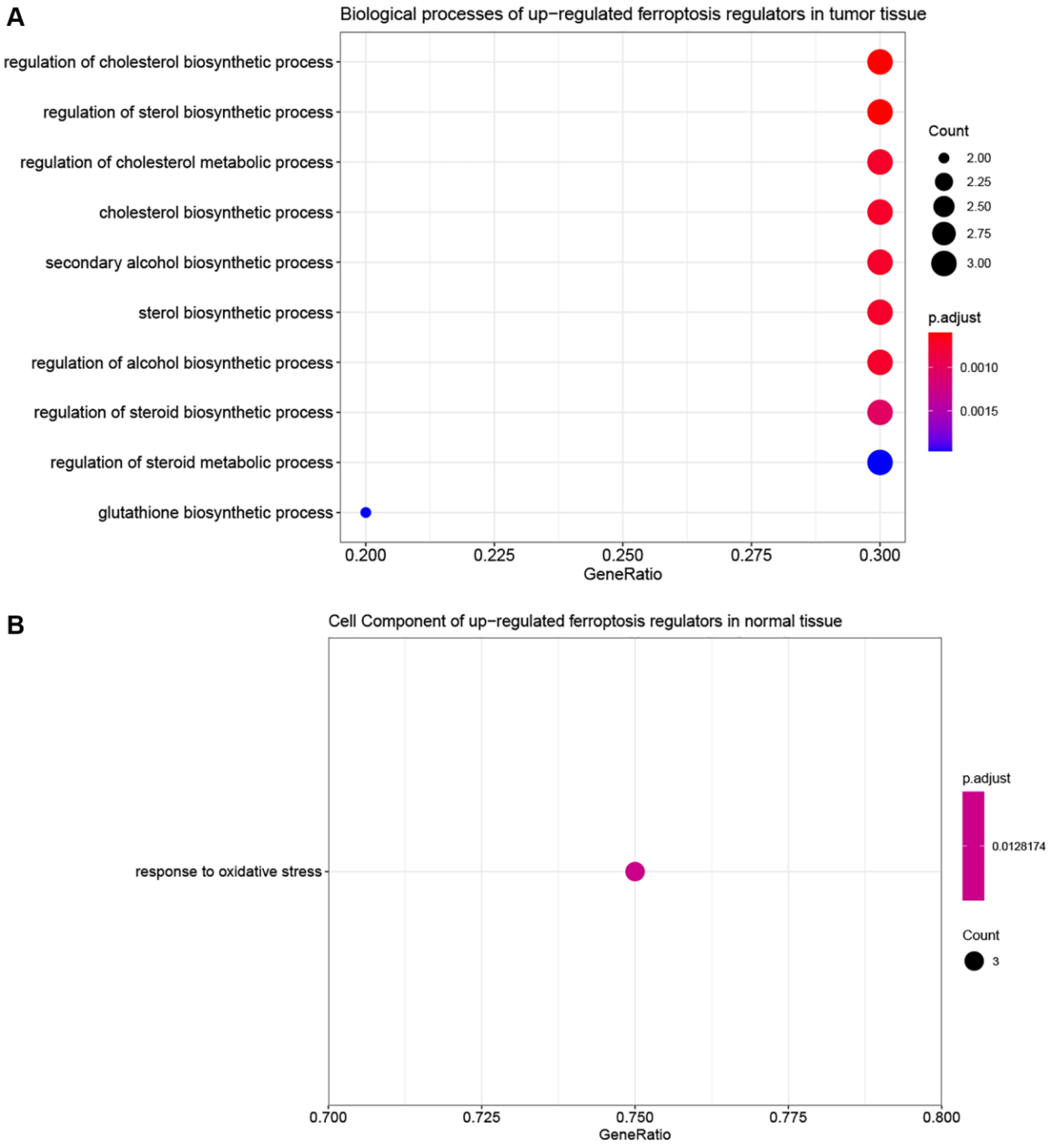

Supplementary Figure 4. Functional enrichment analysis of differentially expressed ferroptosis regulators between normal and tumor tissues. (**A**) Biological processes of upregulated ferroptosis regulators in tumor tissue. (**B**) Cell component of up-regulated ferroptosis regulators in normal tissue.

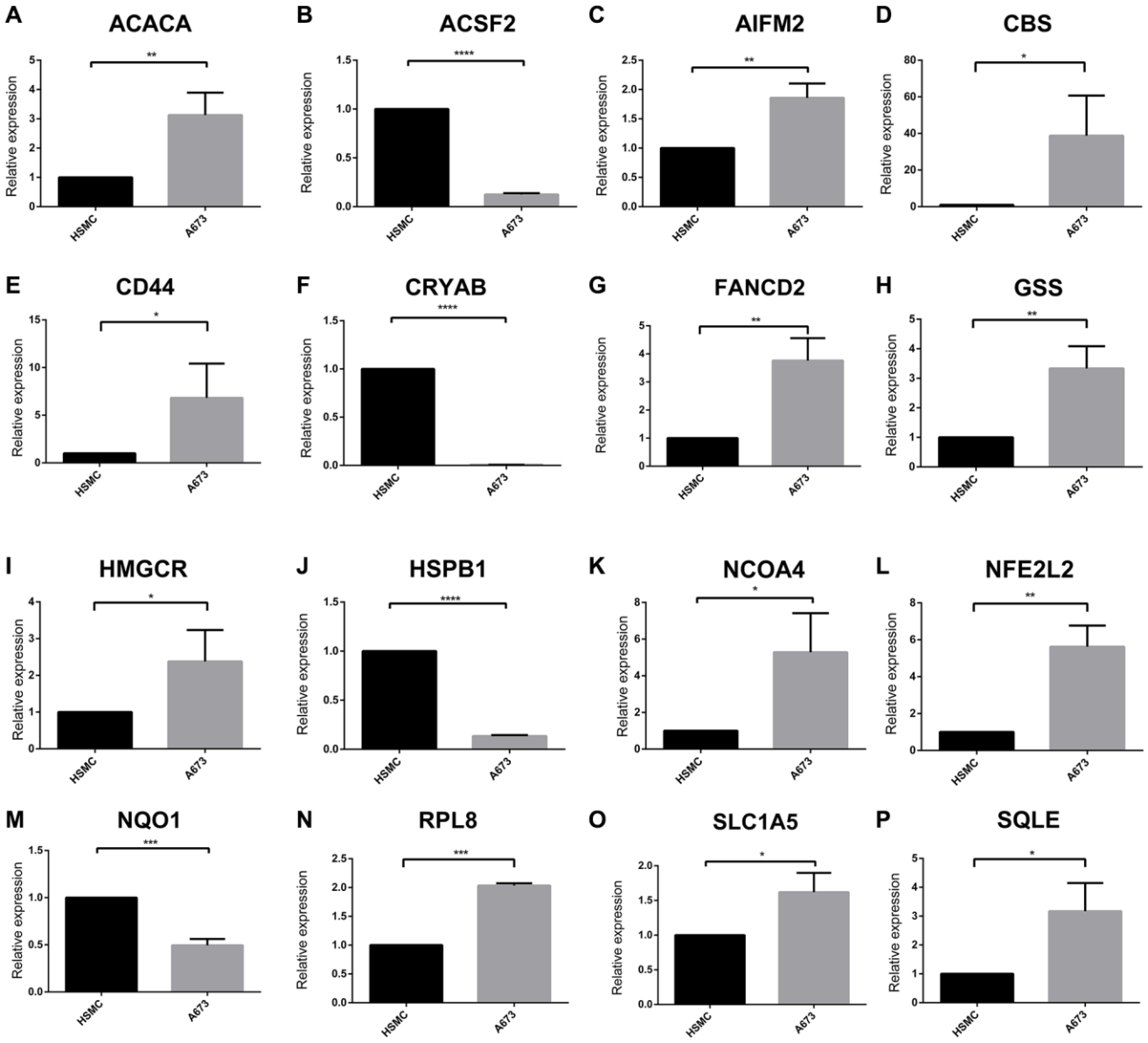

Supplementary Figure 5. Expression of each ferroptosis regulators between STS cell and normal skeletal cell by RT-qPCR. (**A**–**P**) The relative expression of ACACA, ACSF2, AIFM2, CBS, CD44, CRYAB, FANCD2, GSS, HMGCR, HSPB1, NCOA4, NFE2L2, NQO1, RPL8, SLC1A5 and SQLE between tumor and normal cells, respectively. $^{*}p < 0.05$, $^{**}p < 0.01$, $^{***}p < 0.001$, $^{****}p = 0$.

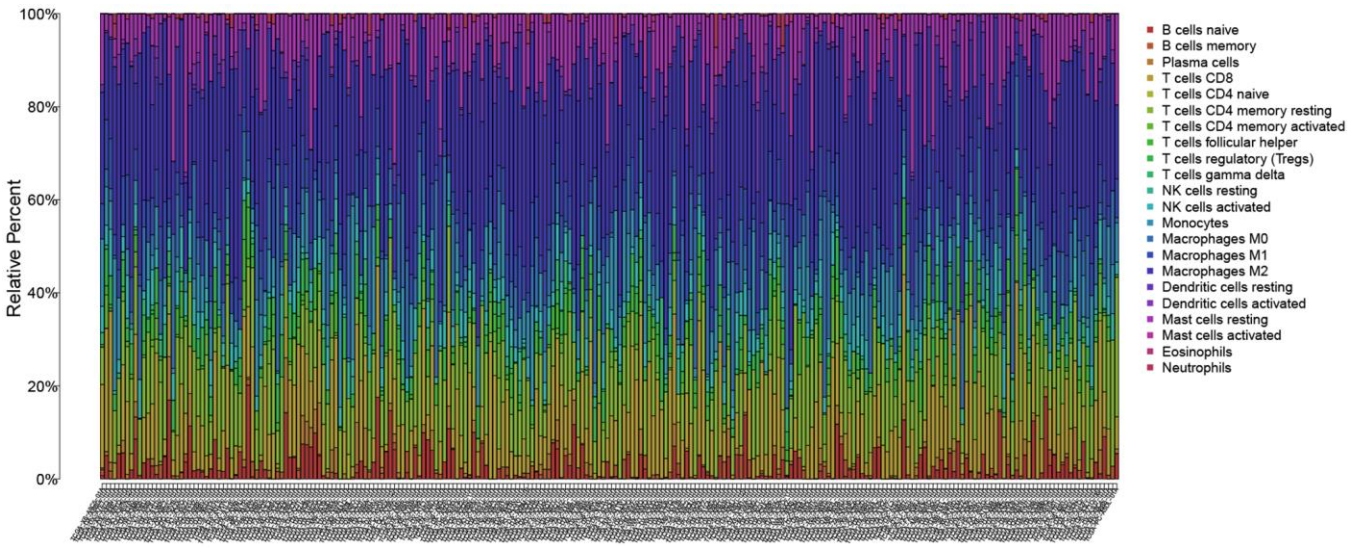

Supplementary Figure 6. Immune infiltration of each sample in TCGA-SARC.

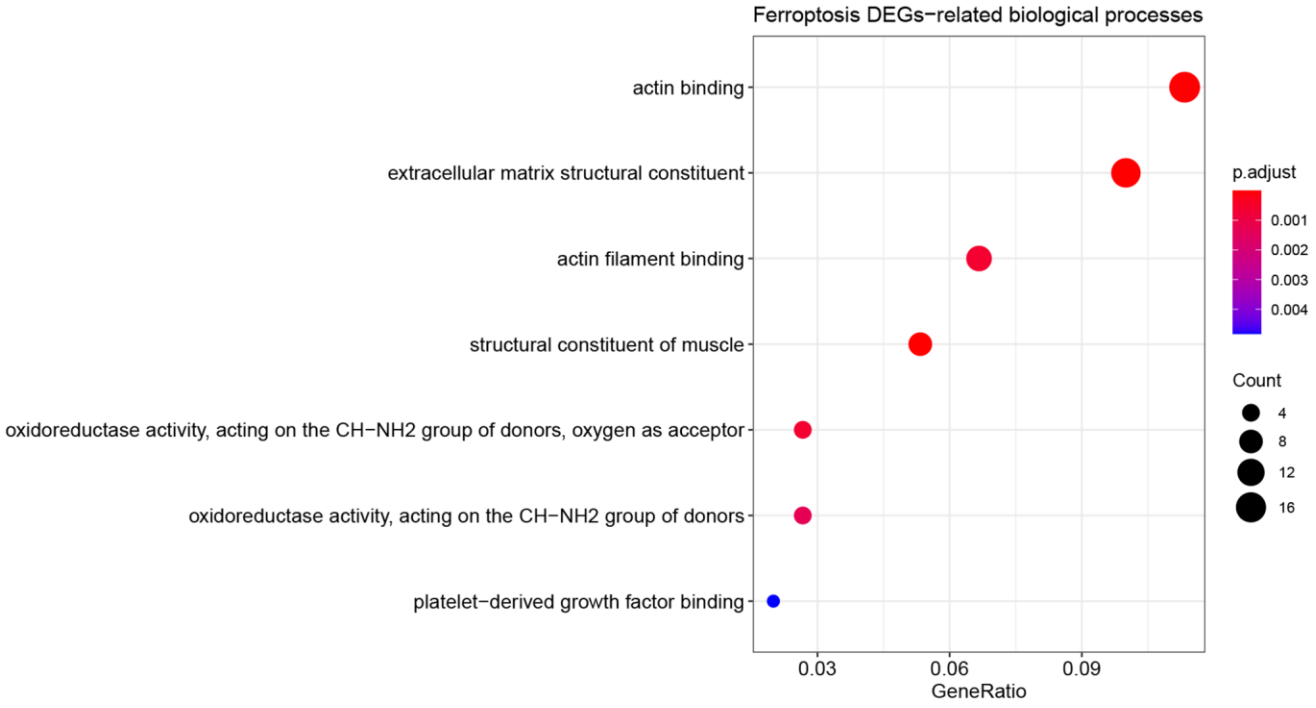

Supplementary Figure 7. Functional enrichment analysis of DEGs between two ferroptosis modification patterns.

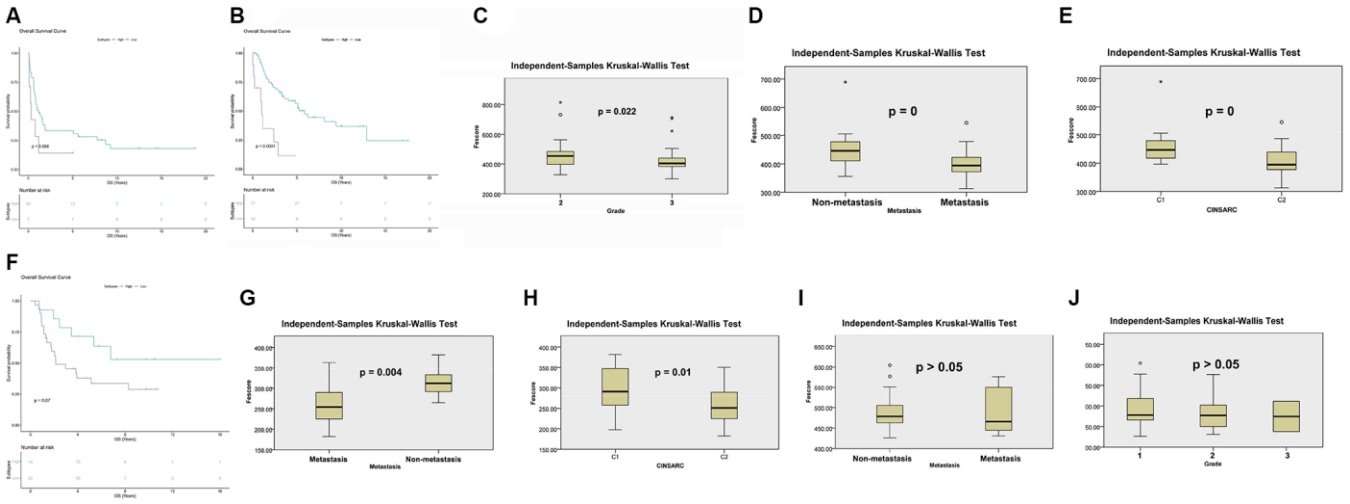

Supplementary Figure 8. Validation of Fescore in different subtypes of STS. (**A**) The survival plot between high and low Fescore group in UDS. (**B**, **C**) The survival plot and grading differences between high and low Fescore groups in LMS. (**D**, **E**) The metastasis and CINSARC index between high and low Fescore groups in SS. (**F**) The survival plot between high and low Fescore group in ES. (**G**, **H**) The metastasis and CINSARC index between high and low Fescore groups in FS. (**I**, **J**) The metastasis and grading between high and low Fescore groups in FS.

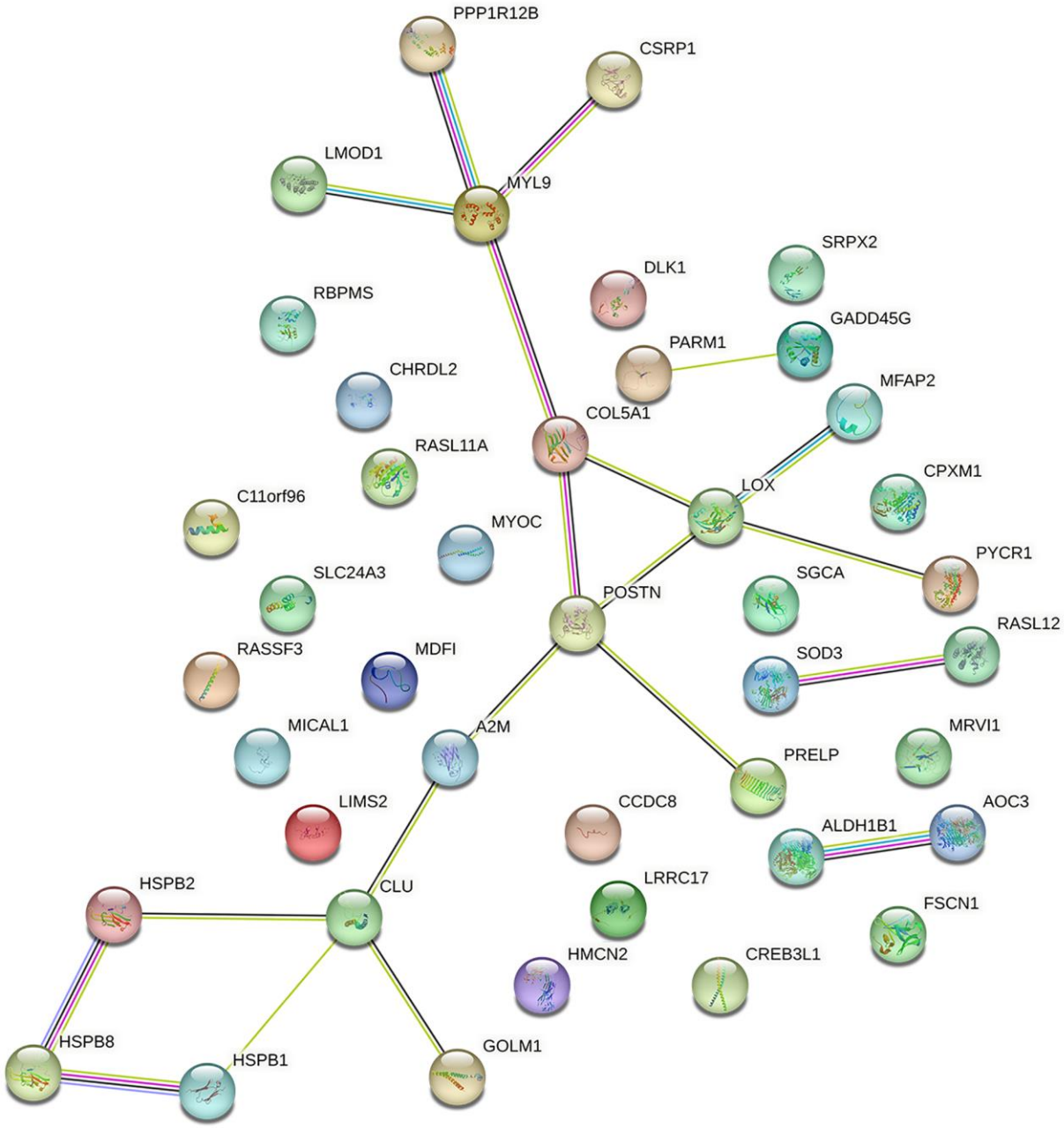

Supplementary Figure 9. Protein-protein interaction analysis of genes that constructed Fescore.

Supplementary Tables

Please browse Full Text version to see the data of Supplementary Table 8.

Supplementary Table 1. Basic information of datasets included in this study.

Accession number/ Source	Platform	Number of patients	Number of samples used in this study	Research object	Survival data
GSE21122	Affymetrix Human Genome U133 Plus 2.0 Array	62	158	Human	OS
GSE35640	Affymetrix Human Genome U133 Plus 2.0 Array	65	56	Human	OS
GSE78220	Illumina RNAseq	28	28	Human	OS
IMvigor210	Illumina RNAseq	348	282	Human	OS
GSE119041	Affymetrix Human Genome U133 Plus 2.0 Array	50	50	Human	OS
GSE40021	Agilent-014850	58	58	Human	NA
GSE159848	Agilent-014850	50	50	Human	OS
GSE159847	Agilent-014850	87	87	Human	OS
GSE17618	Affymetrix Human Genome U133 Plus 2.0 Array	55	44	Human	OS
GSE71118	Affymetrix Human Genome U133 Plus 2.0 Array	312	58	Human	OS
TCGA: SARC	Illumina RNAseq	265	262	Human	OS
TCGA: LAML	Illumina RNAseq	151	132	Human	OS
TCGA: ACC	Illumina RNAseq	79	79	Human	OS
TCGA: CHOL	Illumina RNAseq	45	45	Human	OS
TCGA: BLCA	Illumina RNAseq	430	425	Human	OS
TCGA: BRCA	Illumina RNAseq	1217	1214	Human	OS
TCGA: CESC	Illumina RNAseq	309	296	Human	OS
TCGA: COAD	Illumina RNAseq	512	487	Human	OS
TCGA: UCEC	Illumina RNAseq	583	567	Human	OS
TCGA: ESCA	Illumina RNAseq	173	172	Human	OS
TCGA: GBM	Illumina RNAseq	173	167	Human	OS
TCGA: UCS	Illumina RNAseq	56	54	Human	OS
TCGA: HNSC	Illumina RNAseq	546	545	Human	OS
TCGA: KICH	Illumina RNAseq	89	87	Human	OS
TCGA: KIRC	Illumina RNAseq	607	602	Human	OS
TCGA: KIRP	Illumina RNAseq	321	318	Human	OS
TCGA: DLBC	Illumina RNAseq	48	47	Human	OS
TCGA: LIHC	Illumina RNAseq	424	418	Human	OS
TCGA: LGG	Illumina RNAseq	529	523	Human	OS
TCGA: LUAD	Illumina RNAseq	585	572	Human	OS
TCGA: LUSC	Illumina RNAseq	550	542	Human	OS
TCGA: SKCM	Illumina RNAseq	472	458	Human	OS
TCGA: MESO	Illumina RNAseq	86	84	Human	OS
TCGA: UVM	Illumina RNAseq	80	80	Human	OS
TCGA: OV	Illumina RNAseq	379	378	Human	OS
TCGA: PAAD	Illumina RNAseq	182	181	Human	OS
TCGA: PCPG	Illumina RNAseq	186	186	Human	OS
TCGA: PRAD	Illumina RNAseq	551	551	Human	OS
TCGA: READ	Illumina RNAseq	177	167	Human	OS
TCGA: STAD	Illumina RNAseq	407	381	Human	OS
TCGA: TGCT	Illumina RNAseq	156	139	Human	OS
TCGA: THYM	Illumina RNAseq	121	118	Human	OS
TCGA: THCA	Illumina RNAseq	568	567	Human	OS

Abbreviation: NA: Not applicable.

Supplementary Table 2. The list of ferroptosis regulators.

ACSL4
AKR1C1
AKR1C2
AKR1C3
ALOX15
ALOX5
ALOX12
ATP5MC3
CARS
CBS
CD44
CHAC1
CISD1
CS
DPP4
FANCD2
GCLC
GCLM
GLS2
GPX4
GSS
HMGCR
HSPB1
CRYAB
LPCAT3
MT1G
NCOA4
PTGS2
RPL8
SAT1
SLC7A11
FDFT1
TFRC
TP53
EMC2
AIFM2
PHKG2
HSBP1
ACO1
FTH1
STEAP3
NFS1
ACSL3
ACACA
PEBP1
ZEB1
SQLE

FADS2
NFE2L2
KEAP1
NQO1
NOX1
ABCC1
SLC1A5
GOT1
G6PD
PGD
IREB2
HMOX1
ACSF2

Supplementary Table 3. The sequences of siRNA for LOX (5′ to 3′).

siLOX-1:	GCAGGACTAGATGGAGCAA
siLOX-2:	TGGGACGAGTCAATCAACT
siLOX-3:	GATGGTGGATTACAATGGA

Supplementary Table 4. The prime sequences of all genes.

Genes	Prime sequences (5′–3′)
ACACA-F	AGGTGCCTAGAGGGTTGAAGA
ACACA-R	TCGGCCCTGCTTTACTAGGT
ACSF2-F	GCAGGCAGAGGATTTCAGTTC
ACSF2-R	TTCATGGAGGACGACCAAGG
AIFM2-F	TGATTCTCTGCACCGGCATC
AIFM2-R	GCTGGCTAGTCTGCTCTCAA
CBS-F	GACCAAGTTCCTGAGCGACA
CBS-R	CGGAGGATCTCGATGGTGTG
CD44-F	CTGCCGCTTTGCAGGTGTA
CD44-R	CATTGTGGGCAAGGTGCTATT
CRYAB-F	GGGGTCCTCACTGTGAATGG
CRYAB-R	TTCACGGGTGATGGGAATGG
FANCD2-F	ACATACCTCGACTCATTGTCAGT
FANCD2-R	TCGGAGGCTTGAAAGGACATC
GSS-F	GGTGAGCTATGCCCCATTCA
GSS-R	CACCAGAGCACTGGGCAAT
HMGCR-F	TTCGGTGGCCTCTAGTGAGA
HMGCR-R	GATGGGAGGCCACAAAGAGG
HSPB1-F	GCTTCACGCGGAAATACACG
HSPB1-R	GTGATCTCGTTGGACTGCGT
NCOA4-F	GAGGTGTAGTGATGCACGGAG
NCOA4-R	GACGGCTTATGCAACTGTGAA
NFE2L2-F	TCAGCGACGGAAAGAGTATGA

NFE2L2-R	CCACTGGTTTCTGACTGGATGT
NQO1-F	GACCTTGTGATATTCCAGAGTAAGA
NQO1-R	CCAGGCGTTTCTTCCATCCT
RPL8-F	TGTGATCCGTGGACAGAGGA
RPL8-R	GATCCCGGAAGACCACCTTG
SLC1A5-F	CACGTCCCACCCAGAGAAAC
SLC1A5-R	TGTCCGAAAGCTGGGAGTTC
SQLE-F	GTGCTGGTGTTCCTCTCGCT
SQLE-R	ATTGGTTCCTTTTCTGCGCCT
LOX-F	GGATACGGCACTGGCTACTT
LOX-R	TCTGGGTGTTGGCATCAAGC
GAPDH-F	GCACCGTCAAGGCTGAGAAC
GAPDH-R	TGGTGAAGACGCCAGTGGA

Supplementary Table 5. Functional enrichment analysis of differentially expressed ferroptosis regulators between normal and tumor tissues.

ID	Description	*P*-value	*p*.adjust	*q*-value	geneID	Count
GO:0006979	response to oxidative stress	5.5E-05	0.012817	0.004632	CRYAB/NQO1/HSPB1	3
GO:0045540	regulation of cholesterol biosynthetic process	2.14E-06	0.000601	0.000344	ACACA/HMGCR/SQLE	3
GO:0106118	regulation of sterol biosynthetic process	2.14E-06	0.000601	0.000344	ACACA/HMGCR/SQLE	3
GO:0090181	regulation of cholesterol metabolic process	4.32E-06	0.000742	0.000424	ACACA/HMGCR/SQLE	3
GO:0006695	cholesterol biosynthetic process	7.32E-06	0.000742	0.000424	ACACA/HMGCR/SQLE	3
GO:1902653	secondary alcohol biosynthetic process	7.62E-06	0.000742	0.000424	ACACA/HMGCR/SQLE	3
GO:0016126	sterol biosynthetic process	9.24E-06	0.000742	0.000424	ACACA/HMGCR/SQLE	3
GO:1902930	regulation of alcohol biosynthetic process	9.24E-06	0.000742	0.000424	ACACA/HMGCR/SQLE	3
GO:0050810	regulation of steroid biosynthetic process	1.49E-05	0.001048	0.000599	ACACA/HMGCR/SQLE	3
GO:0019218	regulation of steroid metabolic process	3.32E-05	0.001965	0.001123	ACACA/HMGCR/SQLE	3
GO:0006750	glutathione biosynthetic process	3.5E-05	0.001965	0.001123	GSS/NFE2L2	2
GO:0019184	nonribosomal peptide biosynthetic process	4.39E-05	0.002245	0.001282	GSS/NFE2L2	2
GO:0008203	cholesterol metabolic process	5.85E-05	0.002741	0.001566	ACACA/HMGCR/SQLE	3
GO:1902652	secondary alcohol metabolic process	6.45E-05	0.00279	0.001594	ACACA/HMGCR/SQLE	3
GO:0016125	sterol metabolic process	7.91E-05	0.003176	0.001814	ACACA/HMGCR/SQLE	3
GO:0046165	alcohol biosynthetic process	9.26E-05	0.003468	0.001981	ACACA/HMGCR/SQLE	3
GO:0044272	sulfur compound biosynthetic process	0.000122	0.004167	0.00238	GSS/ACACA/NFE2L2	3
GO:0006694	steroid biosynthetic process	0.00013	0.004167	0.00238	ACACA/HMGCR/SQLE	3
GO:0046890	regulation of lipid biosynthetic process	0.000133	0.004167	0.00238	ACACA/HMGCR/SQLE	3
GO:0010664	negative regulation of striated muscle cell apoptotic process	0.000209	0.006193	0.003538	HMGCR/NFE2L2	2
GO:0042398	cellular modified amino acid biosynthetic process	0.000312	0.008767	0.005008	GSS/NFE2L2	2

GO:1901617	organic hydroxy compound biosynthetic process	0.000337	0.009007	0.005145	ACACA/HMGCR/SQLE	3
GO:0006749	glutathione metabolic process	0.000392	0.009717	0.005551	GSS/NFE2L2	2
GO:0010665	regulation of cardiac muscle cell apoptotic process	0.000406	0.009717	0.005551	HMGCR/NFE2L2	2
GO:0010656	negative regulation of muscle cell apoptotic process	0.000435	0.009717	0.005551	HMGCR/NFE2L2	2
GO:0010662	regulation of striated muscle cell apoptotic process	0.000435	0.009717	0.005551	HMGCR/NFE2L2	2
GO:0010659	cardiac muscle cell apoptotic process	0.00045	0.009717	0.005551	HMGCR/NFE2L2	2
GO:0010658	striated muscle cell apoptotic process	0.00048	0.009991	0.005707	HMGCR/NFE2L2	2
GO:0007568	aging	0.000552	0.011088	0.006334	GSS/HMGCR/NFE2L2	3
GO:0051188	cofactor biosynthetic process	0.000578	0.011199	0.006398	GSS/ACACA/NFE2L2	3
GO:0008202	steroid metabolic process	0.000604	0.011317	0.006465	ACACA/HMGCR/SQLE	3
GO:0006066	alcohol metabolic process	0.000797	0.014442	0.00825	ACACA/HMGCR/SQLE	3
GO:0006790	sulfur compound metabolic process	0.000849	0.014902	0.008513	GSS/ACACA/NFE2L2	3

Supplementary Table 6. Enriched pathways in Fe cluster A.

NAME	ES	NES	NOM *p*-val	FDR *q*-val
HALLMARK_MYOGENESIS	0.634332	3.307229	0	0
HALLMARK_OXIDATIVE_PHOSPHORYLATION	0.604331	3.160266	0	0
HALLMARK_ADIPOGENESIS	0.479207	2.496	0	0
HALLMARK_INTERFERON_ALPHA_RESPONSE	0.503841	2.335555	0	0
HALLMARK_FATTY_ACID_METABOLISM	0.446815	2.273059	0	0
HALLMARK_REACTIVE_OXYGEN_SPECIES_PATHWAY	0.560496	2.267417	0	0
HALLMARK_BILE_ACID_METABOLISM	0.445523	2.114106	0	1.14E-04
HALLMARK_ESTROGEN_RESPONSE_LATE	0.389252	2.058489	0	3.29E-04
HALLMARK_UV_RESPONSE_UP	0.398036	2.016938	0	2.93E-04
HALLMARK_HEME_METABOLISM	0.357601	1.886102	0	8.47E-04
HALLMARK_INTERFERON_GAMMA_RESPONSE	0.355599	1.861583	0	8.33E-04
HALLMARK_KRAS_SIGNALING_DN	0.349546	1.806281	0	0.00131
HALLMARK_XENOBIOTIC_METABOLISM	0.335465	1.736298	0.0020408	0.002037
HALLMARK_ESTROGEN_RESPONSE_EARLY	0.321899	1.661753	0	0.003715
HALLMARK_PEROXISOME	0.35326	1.639113	0.001996	0.004375
HALLMARK_APICAL_JUNCTION	0.311443	1.632621	0	0.00443
HALLMARK_COAGULATION	0.304079	1.484184	0.0105042	0.018053
HALLMARK_CHOLESTEROL_HOMEOSTASIS	0.331957	1.471765	0.0347648	0.01924
HALLMARK_P53_PATHWAY	0.272602	1.404251	0.0217822	0.033998
HALLMARK_SPERMATOGENESIS	0.228275	1.128314	0.246124	0.227237

Supplementary Table 7. Enriched pathways in Fe cluster B.

NAME	ES	NES	NOM *p*-val	FDR *q*-val
HALLMARK_MYC_TARGETS_V2	−0.71611	−3.08285	0	0
HALLMARK_TGF_BETA_SIGNALING	−0.68269	−2.83247	0	0
HALLMARK_UNFOLDED_PROTEIN_RESPONSE	−0.55997	−2.68873	0	0
HALLMARK_MYC_TARGETS_V1	−0.5152	−2.67385	0	0
HALLMARK_PROTEIN_SECRETION	−0.55427	−2.59826	0	0
HALLMARK_EPITHELIAL_MESENCHYMAL_TRANSITION	−0.48943	−2.56332	0	0
HALLMARK_G2M_CHECKPOINT	−0.4862	−2.55363	0	0
HALLMARK_UV_RESPONSE_DN	−0.45711	−2.2864	0	0
HALLMARK_KRAS_SIGNALING_UP	−0.42344	−2.21573	0	0
HALLMARK_NOTCH_SIGNALING	−0.59168	−2.17589	0	0
HALLMARK_MITOTIC_SPINDLE	−0.4068	−2.15244	0	0
HALLMARK_WNT_BETA_CATENIN_SIGNALING	−0.54391	−2.14052	0	0
HALLMARK_MTORC1_SIGNALING	−0.4043	−2.11334	0	0
HALLMARK_ANGIOGENESIS	−0.55215	−2.08895	0	0
HALLMARK_E2F_TARGETS	−0.39287	−2.08114	0	0
HALLMARK_GLYCOLYSIS	−0.38931	−2.03895	0	0
HALLMARK_INFLAMMATORY_RESPONSE	−0.37657	−1.96033	0	0.00E+00
HALLMARK_TNFA_SIGNALING_VIA_NFKB	−0.34199	−1.82698	0	2.39E-04
HALLMARK_ALLOGRAFT_REJECTION	−0.33756	−1.7869	0.0020534	0.000825
HALLMARK_HEDGEHOG_SIGNALING	−0.47323	−1.76656	0.0094162	0.001076
HALLMARK_ANDROGEN_RESPONSE	−0.36871	−1.71922	0.0020747	0.001525
HALLMARK_COMPLEMENT	−0.3241	−1.7179	0	0.001456
HALLMARK_IL2_STAT5_SIGNALING	−0.32191	−1.70063	0	0.001571
HALLMARK_HYPOXIA	−0.30643	−1.62027	0.0019342	0.00444
HALLMARK_APOPTOSIS	−0.29261	−1.49237	0.001992	0.013702
HALLMARK_APICAL_SURFACE	−0.35631	−1.40262	0.0677656	0.031103
HALLMARK_DNA_REPAIR	−0.27639	−1.39083	0.0291971	0.03286
HALLMARK_IL6_JAK_STAT3_SIGNALING	−0.29632	−1.37348	0.0384615	0.037574

Supplementary Table 8. The full list of DEGs between Fe cluster A and B.

Supplementary Table 9. Functional enrichment analysis of DEGs between two ferroptosis modification patterns.

ID	Description	*p*-value	*p*.adjust	*q*-value	geneID	Count
GO:0005201	extracellular matrix structural constituent	8.44286E-12	3.05E-09	2.81E-09	POSTN/COL1A1/COL5A1/COL12A1/ SBSPON/DCN/FBLN2/NPNT/ HMCN2/MXRA5/SRPX2/LUM/ MFAP2/PCOLCE/PRELP	15
GO:0008307	structural constituent of muscle	4.38733E-09	7.92E-07	7.3E-07	MYL9/CSRP1/SYNM/PDLIM3/ MYH11/TPM1/TPM2/MYOM1	8
GO:0003779	actin binding	1.51403E-07	1.82E-05	1.68E-05	CAP2/SORBS1/ADD3/CNN1/SYNPO2/ FLNA/LMOD1/PDLIM3/MYH11/MYLK/ MICAL1/FSCN1/TAGLN/TMOD1/ TPM1/TPM2/MYOM1	17

GO:0051015	actin filament binding	7.37154E-06	0.000602	0.000555	ADD3/FLNA/MYH11/MICAL1/FSCN1/ TAGLN/TMOD1/TPM1/TPM2/MYOM1	10
GO:0016641	oxidoreductase activity, acting on the CH-NH2 group of donors, oxygen as acceptor	8.33687E-06	0.000602	0.000555	LOX/MAOA/MAOB/AOC3	4
GO:0016638	oxidoreductase activity, acting on the CH-NH2 group of donors	2.1615E-05	0.001301	0.001198	LOX/MAOA/MAOB/AOC3	4
GO:0048407	platelet-derived growth factor binding	9.36937E-05	0.004832	0.004452	COL1A1/COL5A1/PDGFRA	3

Supplementary Table 10. Cmap analysis for DEGs.

Cmap name	Mean	*n*	Enrichment	*p*	Specificity	Percent non-null
Doxylamine	−0.655	5	−0.888	0.00006	0	100
Sulfadimethoxine	−0.399	5	−0.851	0.00022	0	60
Carteolol	−0.266	4	−0.837	0.00123	0	50
3-acetamidocoumarin	−0.352	4	−0.837	0.00125	0.026	50
PHA-00851261E	0.421	8	0.627	0.00154	0	75
Sulfaquinoxaline	−0.646	3	−0.899	0.00192	0.0062	100
AH-6809	−0.707	2	−0.961	0.0033	0.0056	100
Harmine	0.31	4	0.796	0.00342	0.0076	50
Karakoline	−0.371	6	−0.653	0.00475	0	50
Difenidol	0.455	3	0.863	0.00481	0.0152	66
Sulfadiazine	−0.528	5	−0.684	0.00717	0.0263	80
Isoniazid	−0.388	5	−0.672	0.00885	0.0497	60
Cefotiam	−0.282	4	−0.741	0.00891	0.0065	50
Hydrocortisone	0.382	3	0.834	0.00915	0	66
Etiocholanolone	−0.402	6	−0.612	0.01124	0.1948	66
Mafenide	−0.291	5	−0.654	0.0122	0.018	60
STOCK1N-35874	0.649	2	0.92	0.01272	0.0435	100
Proscillaridin	0.491	3	0.813	0.01302	0.0842	66
Withaferin A	0.624	4	0.71	0.01452	0.1947	75
16-phenyltetranorprostaglandin E2	−0.535	4	−0.708	0.0151	0.0298	75
Sitosterol	0.261	4	0.7	0.01667	0.0172	50
PF-00539745-00	−0.384	3	−0.798	0.01703	0.0815	66
Puromycin	0.474	4	0.695	0.01818	0.2472	75
Ticarcillin	0.366	3	0.789	0.01889	0.0133	66
Flunarizine	0.35	4	0.691	0.01898	0.034	50
Gliquidone	0.519	4	0.69	0.01932	0	75
Cyproterone	0.328	4	0.677	0.02367	0.024	50
Alverine	−0.354	4	−0.672	0.02586	0	75
Clenbuterol	−0.407	5	−0.598	0.03004	0.0397	60
Oxybenzone	−0.369	4	−0.657	0.03191	0.0986	50
Practolol	0.258	4	0.649	0.03599	0.0259	50

Abamectin	−0.493	4	−0.646	0.0375	0.0617	75
Diazoxide	−0.356	5	−0.574	0.04189	0.061	60
PHA-00767505E	0.433	4	0.636	0.04307	0.0387	75
Harmalol	−0.479	3	−0.724	0.04333	0.052	66
Sparteine	0.481	4	0.635	0.04345	0.0072	75
Econazole	0.242	4	0.632	0.04552	0.1949	75
Nialamide	0.429	4	0.63	0.04677	0.036	75
5255229	0.34	2	0.847	0.0472	0.0474	50
Indoprofen	−0.314	4	−0.626	0.04852	0.1333	50
Colecalciferol	−0.409	4	−0.625	0.04886	0.0272	75
Cinnarizine	0.549	4	0.625	0.04933	0.0584	75

Supplementary Table 11. Full list of 43 prognostic DEGs.

	cox_HR
LIMS2	0.382144
AOC3	0.481967
SOD3	0.495754
C11orf96	0.543024
HMCN2	0.543768
A2M	0.546305
GADD45G	0.554395
HSPB8	0.573024
CLU	0.573242
MYOC	0.582298
RASL11A	0.582661
CSRP1	0.59421
MRVI1	0.618517
PARM1	0.622781
RASSF3	0.629226
SLC24A3	0.634694
PPP1R12B	0.634896
CHRDL2	0.641911
HSPB2	0.642656
RBPMS	0.645255
RASL12	0.649648
SGCA	0.649931
MICAL1	0.652491
LMOD1	0.65268
HMGN2P19	0.65459
MYL9	0.663697
HSPB1	0.663706
ALDH1B1	0.666453
PRELP	0.667319
DLK1	1.499914
POSTN	1.530762
COL5A1	1.53084

SRPX2	1.543947
FSCN1	1.587907
CREB3L1	1.594449
CCDC8	1.631176
GOLM1	1.63245
CPXM1	1.658367
MDFI	1.665139
PYCR1	1.732861
LOX	1.819126
MFAP2	1.903821
LRRC17	2.177627